HIGH TEMPERATURE SUPERCONDUCTING $YBa_2Cu_3O_{7-x}$ TRANSITION EDGE BOLOMETERS (TEBs) FOR INFRARED REGION

A Thesis submitted to
The Graduate School of Engineering and Science of
İzmir Institute of Technology
in Partial Fulfillment of the Requirements for the Degree of

MASTER OF SCIENCE

in Physics

by

Hacı Yusuf GÜNEL

November 2008
İZMİR

We approve the thesis of **Hacı Yusuf GÜNEL**

_____

Prof. Doğan ABUKAY
Supervisor

_____

Assist. Prof. Yusuf SELAMET
Committee Member

_____

Assist. Prof. Ali BOZBEY
Committee Member

28 November 2008
Date

_____

Prof. Dr. Durmuş Ali DEMİR
Head of the Physics Department

_____

Prof. Hasan BÖKE
Dean of the Graduate School of Engineering and Sciences

ACKNOWLEDGEMENTS

It is my pleasure to acknowledge the many people who helped me directly or indirectly during this work.

First of all, I would like to thank my supervisor Prof.Dr.Doğan ABUKAY for his support and encouragement throughout this work.

My lab mate Barış Pekerten deserves a big “Thank you”, not only for sharing his deep scientific knowledge with me but also for being a good friend.

I would also like to thank Dr. İlbeyi Avcı for being a great mentor and Dr. Ali Bozbey for sharing his experiences with me whenever I needed.

Furthermore, I would like to thank all my friends in IYTE for creating a nice environment in the physics building, especially during the long, long nights.

Finally, it is my pleasure to express my sincere gratitude to my family for always supporting and encouraging me.

This work partially supported by IYTE-BAP11.

ABSTRACT

HIGH TEMPERATURE SUPERCONDUCTING $YBa_2Cu_3O_{7-x}$ TRANSITION EDGE BOLOMETERS (TEBs) FOR INFRARED REGION

The thesis focuses on electrical and bolometric characterization of high temperature superconducting YBCO transition edge bolometers. In this study, superconducting YBCO thin films grown on MgO, $LaAlO_3$ and $SrTiO_3$ substrates were first characterized structurally via x-ray diffraction and scanning electron microscopy. They then were patterned into bolometers and their electrical and bolometric characterizations were carried out. The results of these characterizations were fitted to the RC model. In addition, figures of merit for these devices, such as noise equivalent power (NEP) and detectivity, were measured and calculated.

During this work, the patterning process was carried out by standard photolithographic processes and chemical etching. We have also investigated the effect of dimensions of our devices on the performance of bolometers. The electrical and bolometric characterizations comprised of resistance versus temperature (R-T), amplitude of response versus temperature, amplitude of response versus chopping frequency (A-F) and noise voltage measurements. Finally, the performance of our devices were compared to literature and found to be similar to or better than those of similar devices in literature.

ÖZET

KIZILÖTESİ BÖLGESİ İÇİN YÜKSEK SICAKLIK ÜSTÜNİLETKEN $YBa_2Cu_3O_{7-x}$ GEÇİŞ KENAR BOLOMETRELERİ

Bu çalışmanın temel amacı yüksek sıcaklık $YBa_2Cu_3O_{7-x}$ (YBCO) süperiletken kenar geçiş bolometrelerinin elektriksel ve bolometrik özelliklerini araştırmaktır. Bu çalışmada MgO, $LaAlO_3$ ve $SrTiO_3$ alt taşlar üzerine epitaksiyel olarak büyütülmüş YBCO ince filmler ilk olarak x-ışını kırınımı ve elektron mikroskobu ile yapısal olarak incelendi. Daha sonra bu filmler üzerine bolometre desenleri yapılarak elektriksel ve bolometrik karakterizasyonları yapıldı. Alınan sonuçlar RC modeline fit edildi. Bunlara ek olarak bu cihazların hassaslık ve ışık alınganlıkları gibi performans karakterizasyonları (figures of merit) yapıldı. Bu tezde desenleme ve bolometrik karakterizasyon için farklı alt taşlar üzerine büyütülmüş malzemeler kullanıldı. Malzemelerin elektrik ve bolometrik karakterizasyonundan sonra alınan sonuçlar RC modeli ile karşılaştırıldı. Ayrıca kenar geçiş bolometrelerinin performans karakterizasyonu için hassaslık (sensitivity, noise equivalent power) veya gürültü ve ışığı algılama kabiliyeti (Detectivity) ölçümleri (figures of merit) yapıldı.

Bu çalışma sırasında desenleme işlemleri standart fotolitografik ve kimyasal oyma (etch) yöntemleri ile yapıldı. Farklı fiziksel boyutlarda dizayn edilen cihazların bolometre performansları üzerindeki etkileri araştırıldı. Elektriksel ve bolometrik karakterizasyon için direnç – sıcaklık (R-T), tepki genliği – sıcaklık (A-T), tepki genliği – kesme frekansı (A-F) ve her aygıt için sabit kesme frekansında gürültü voltaj ölçümleri alındı. Son olarak gürültü ölçümleri kullanılarak aygıtların ışığı algılama kabiliyetleri hesaplandı ve sonuçlar literatür ile karşılaştırıldı.

To my Family and Friends

TABLE OF CONTENTS

LIST OF FIGURES

Figure **Page**

LIST OF TABLES

CHAPTER 1

INTRODUCTION

High temperature superconducting $YBa_2Cu_3O_{7-\delta}$ (YBCO) transition edge bolometer (TEB) is a type of thermal radiation detector operated at the midpoint of superconducting transition region. The detector, or bolometer, consists of two main elements which are the radiation absorber and the thermometer with a heat capacity C. These elements are kept at a constant temperature T_0 via a connecting weak thermal link having a heat conductivity G to a heat bath. At this constant temperature, the detector is biased with a constant current that would avoid thermal runaway and the voltage of the detector is sensed before illuminating radiation (in the case of voltage bias, the current is sensed). Radiation is then allowed to fall on the detector, causing the temperature of the detector to increase by δT, causing an increase in the resistance of the detector.

Thermal detectors are classified into five groups which are bolometers, thermopiles, pyroelectric detectors, Golay cells and superconducting detectors (Dereniak and Boreman 1996). Thermopiles are temperature to electric potential difference transducers, pyroelectric detectors are based on surface charge change (capacitance), Golay cells depend on gas pressure and bolometers are based on resistance change. All of these detectors have high sensitivities in different radiation wavelength regions. Superconducting bolometers have the highest sensitivity above 20 μm among these detectors. Furthermore, high temperature superconducting bolometers have higher sensitivity than room temperature detectors at above 20μm wavelength regimes (Hu and Richards 1989).

Many materials can be used for fabricating bolometers. The first bolometer, known as Langley's Bolometer (NASA Earth Observatory 2000), was made with two platinum strips (whose the details will mentioned in the next chapter). Due to having a variety of thermal detector types based on different materials, they have wide application areas such as medical imaging, astronomy, millimeter wave and THz detection, single photon detection and x-ray detectors (Bozbey 2006). Superconducting detectors have high performance at these application areas. Usually, junction based low

temperature superconductors are used for these applications. Thermal imaging applications of high temperature superconductors, are also available (Rahman 2006).

High temperature superconductors (HTS) were discovered long after the discovery of superconductivity (Bednorz and Muller 1986). Soon after, a new and promising perovskite superconductor, YBCO, was discovered (Wu, et al. 1987) which has a superconducting transition temperature at about 92K. This discovery is very important because of having a T_c above liquid nitrogen temperature (77K) which implies that its use and research does not require complex and expensive systems. As a consequence, high temperature superconducting YBCO has been widely investigated. It has many large and small scale application areas, one of which is high temperature superconducting YBCO transition edge bolometers, which is the objective of this thesis

The YBCO compound is the most studied and best characterized material among the CuO based HTS materials. It has good bolometric performance relative to the other HTS materials. Generally, HTSs have a complex structure and they are not easy to fabricate epitaxially with conventional growth techniques due to having Cu-O planes, but YBCO cam be grown epitaxially with relative ease. YBCO has an orthorhombic structure when optimally doped ($\delta=0$) and it is an insulator when $\delta=1$. The change in oxygen content from $\delta=0$ to $\delta=1$ results in a phase transition in the material from a tetragonal antiferromagnetic insulator to an orthorhombic metal exhibiting superconductivity when stoichiometry reaches about 6.4 (Mischke 2003). Farrel reported an anisotropy of YBCO between the ab plane and c axis. The details of the crystal structure of YBCO will be given in the next chapter (Farrell, et al. 1990).

Superconducting materials have many application areas which are generally classified into two groups as large and small scale applications. Power cables, current limiters, flywheels and few others are examples of large scale applications while small scale applications include Josephson junctions, superconducting quantum interference devices (SQUIDs), superconducting flux qubits, rapid single flux quantum (RSFQ), stripline resonators and transition edge bolometers (TEBs).

Small scale applications of superconducting materials such as YBCO require thin films and an appropriate substrate. In order to make transition edge bolometers, further requirements on substrates are present. Substrate requirement for growth of high temperature superconductors is reviewed by Wördenweber. He enumerated the requirements on the substrates as follows: Crystallographic lattice match between HTS

film and substrate, similar thermal expansivities of HTS and substrate, no chemical interaction at the interface between HTS and substrate, and finally, suitable polished surface and stable and reasonably robust product (Wördenweber 1999). In addition, the physical, thermal and optical properties of substrates of the HTSs can affect the performance of bolometers significantly.

One of the most important steps of fabrication of YBCO bolometers is choosing an appropriate substrate with an appropriate thermal conductance G and having an appropriate heat capacity C (Richards 1994). One of the key parameter of bolometers is thermal conductance because it changes with temperature. The magnitude of thermal conductance is very important because it needs to be known for most of theoretical calculations such as responsivity. M. Fardmanesh investigated many measurement methods for thermal conductance among which was the Joule heating method, which we utilized (Fardmanesh, et al. 1995). On the other hand, the speed and magnitude of response mainly depends on heat capacitance and thermal conductance of substrate. The response of bolometers increases when it has a large heat capacity but in that case the speed of bolometers decreases or time constant τ increases (τ=C/G) (Richards, et al. 1989, Khrebtov 1999, Kreisler 2000, Kruse 1990).

Furthermore, the thermal conductance between substrate/film interface and substrate/cold head interface also play important roles on the performance of bolometers. In order to observe the effect of substrate/film interface on the amplitude of response, a much higher chopping frequency range on the order of MHz is needed. At low chopping frequency range, the heat which is created by radiation can diffuse to the cold head. In this case the thermal conductance between substrate and cold head becomes dominant and substrate/film thermal conductance can be negligible (Fardmanesh, et al. 1995). In this work we have investigate the performance of bolometers at the low chopping frequency range.

In this thesis, we have characterized YBCO thin films by x-ray diffraction and scanning electron microscopy while electrical and bolometric characterizations consisted of resistance versus temperature, amplitude of response versus temperature, amplitude of response versus chopping frequency and noise measurements. In addition, we have used the RC model in order to fit amplitude of response versus chopping frequency measurements.

The performance characterizations employed were the measurement and calculation of optical responsivity, noise equivalent power (NEP) and detectivity (D^*). The responsivity of a bolometer is defined as the amount of input power radiation per measured signal voltage in the units of V/W. The NEP is defined as the responsivity of bolometer per voltage noise and detectivity can be calculated with the knowledge of NEP and the absorption area, (A) of the bolometer and is given by $\sqrt{A}/NEP$. The details of performance measurements of bolometers are given in the discussion chapter of this thesis.

This thesis consists of five chapters. The theoretical background of transition edge bolometers (TEBs) is given in the 2nd chapter, which is mainly focused on TEBs made with high temperature superconducting YBCO thin films. The details of experimental techniques are given in the 3rd chapter. The results and discussions are given in the 4th chapter and conclusion of the thesis is given in the 5th chapter.

CHAPTER 2

TRANSITION EDGE BOLOMETERS (TEBs)

2.1. Infrared (IR) Radiation

Infrared radiation was discovered in 1800 by Frederick William Herschel. He used a thermometer for detecting IR radiation. He passed sunlight through a prism to separate the light into its spectrum as usual. He then connected the thermometer below the red light and observed that the temperature was increasing. He thus surmised the reason was invisible radiation, which he dubbed "infrared," using the Latin word "infra" for "below."

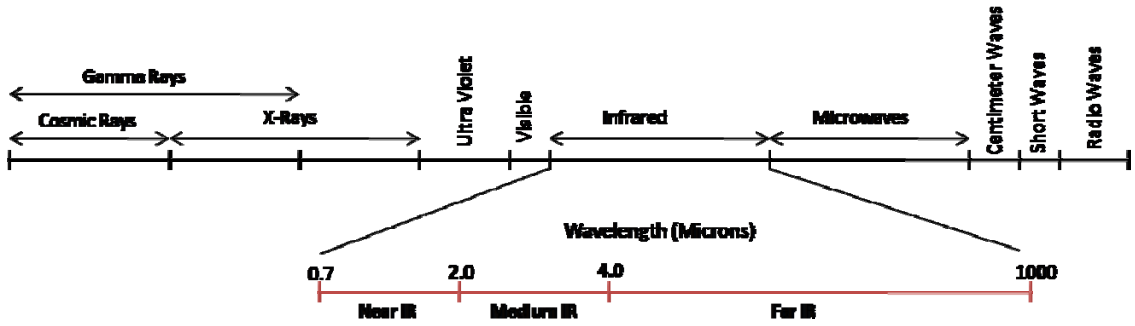

Figure 2. 1. Radiation spectrum chart and inset shows the Near IR, Mid-IR and Far IR regions.

Infrared radiation is usually classified into three regions, which are near, mid and far infrared (IR) as shown in Figure 1. There is no well defined boundary between these regions. Usually, near IR range is taken to be between 0.7μm-2μm, mid IR range between 2μm-4μm and Far IR range between 4μm-1000μm.

According to the Planck's radiation law, all objects at nonzero temperatures can radiate infrared radiation. Even if not a perfect blackbody, almost any object at temperatures higher than 0^{o}K radiates IR light to some degree.

2.2. Basic Operating Principle of Bolometers

Bolometers are a type of thermal detector. The first bolometer, known as Langley's Bolometer, was invented in 1878 by Samuel Pierpont Langley. It had a very basic design: he used two platinum strips, one of them covered with lampblack and the other shielded from the sun light. The first one was exposed to sunlight. The strips formed two branches of a Wheatstone bridge which was fitted with a sensitive galvanometer and connected to a battery. Electromagnetic radiation falling on the exposed strip would heat it and change its resistance, the circuit thus effectively operating as a temperature to resistance transducer (NASA Earth Observatory 2000).

Due to the simple principle of Langley's bolometer, temperature dependence of resistance has been widely studied. Hence, it is relatively easy to select a material for detector design. Consequently, it is possible to find various kinds of radiation detectors with different purposes and mechanisms, outlined in table 2.1.

Table 2.1. Thermal detector types and their mechanism

Detector Type	Mechanism
Bolometers	Resistance
Thermopile	Voltage
Pyroelectric	Capacitance / Ferroelectric Material
Golay cell	Gas Pressure
Superconductor	Resistance

Table 2.1 shows various kinds of thermal detectors and their mechanisms. ***Bolometers*** are a type of thermal detector whose resistance is a function of temperature and which has ability to detect radiation with broad wavelength (from visible to far infrared) (Richards 1994). Basically, it consists of two parts, i.e. the absorption element and the thermometer. When radiation strikes the absorbing element, the temperature of bolometer increases, leading to a change in resistance. Consequently, this temperature change can tell us how much radiant energy is falling on the bolometer. ***Thermopile sensors*** produce electrical voltage from optical radiation. They are a junction of two unlike metals and do not need to be biased. In order to increase voltage output, these

sensors usually consist of a series of thermocouples called a thermopile. Thermopile detectors are relatively slow responding devices and are typically used with chopped radiation at frequencies less than 25 Hz (Herwaarden and Duyn 1989).

In ***pyroelectric sensors,*** a change in temperature creates a change in polarization. Electrical polarization change is related to a surface-charge change with respect to time resulting in an electrical current. Thus, a pyroelectric detector produces current only as it experiences a temperature rise or fall (Dereniak and Boreman 1996).

Golay Cell detectors consist of three parts: the gas chamber, optical readout and electrical readout. An infrared radiation absorbing element is placed in a chamber filled with pressurized gas. An infrared transmitting window allows radiation into the chamber. When the radiation absorbed, it heats up the absorber and by convection heats the gas in the chamber. The increased temperature of the gas results in increased pressure in the chamber. By the ideal gas law ($PV \sim T$), if the volume is constant, the pressure and temperature are directly related. The chamber volume is controlled by a solid structure completely surrounded except for a small flexible membrane with a reflecting coating on the exterior of the membrane, which acts as a mirror. As the pressure changes, the mirror flexure also changes. The amount of distortion is sensed by a separate optical system consisting of a light source and photo detector. Today, it is used for very far infrared ranges ($\lambda > 300\mu m$) (Dereniak and Boreman 1996).

Superconductor transition edge sensors operate in the middle of the transition region between normal and superconducting state. In this region, resistance is highly dependent on temperature. The temperature of the device has to be constant at that region. When the absorbing element of the device is illuminated by radiation, the temperature of the device will change and also resistance of device will change due to the radiation. These types of detectors are more sensitive than room temperature detectors such as golay cells and pyroelectric detectors. The rest of this thesis will primarily focus on this type of bolometer.

Superconducting radiation detectors are classified into two groups, which are quantum detectors and bolometric detectors (Rahman 2006). *Quantum detectors* are junction based detectors and usually consist of direct SIS tunnel junction detectors, heterodyne SIS tunnel junction detectors and superconducting quantum well detectors. Superconducting *bolometric detectors* can be classified as transition edge bolometers (TEBs), heterodyne hot electron microbridge detectors and superheated grain detectors.

The objective of this work is to investigate high-T_c superconducting epitaxial thin film $YBa_2Cu_3O_{7-\delta}$ transition edge bolometers.

As shown in figure 2.2, bolometers consist of two main parts which are the radiation absorbing element and the thermistor. Both of them are connected via a weak thermal link ***G*** to a heat bath kept at a constant temperature T_0. When radiation is illuminated on the absorbing element, the temperature of the thermistor increases by ΔT, thus causing to increased resistance of bolometer, which then can be measured by standard means.

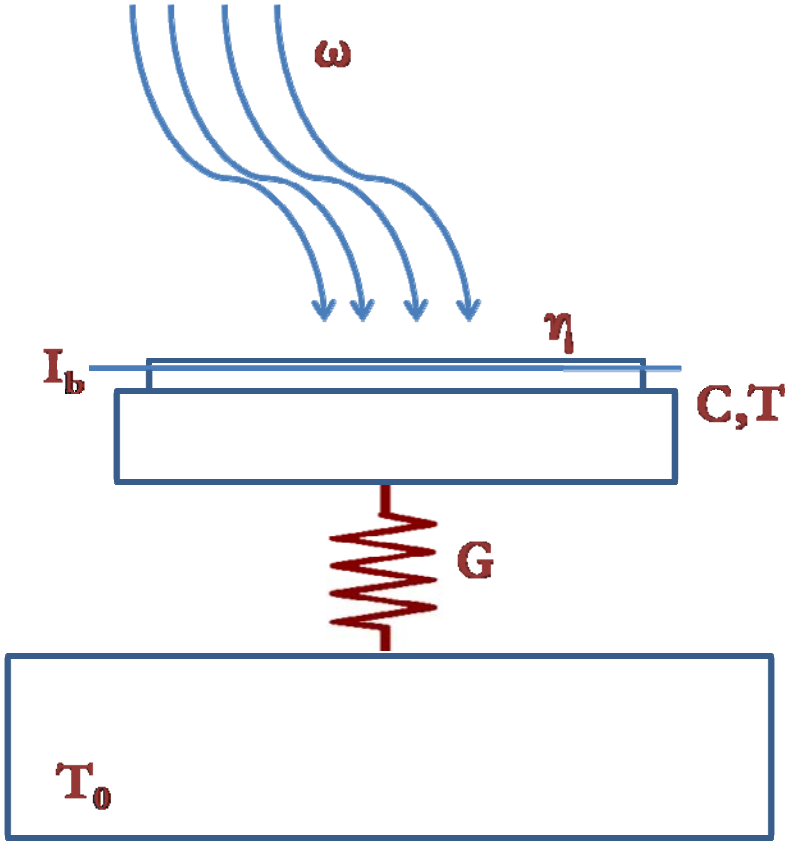

Figure 2. 2. Schematic diagram of operation of transition edge bolometer (TEB)

Other important parameters of the system include the heat capacity of the bolometer, ***C***, and the chopping frequency of the incoming radiation, ω, and the thermal time constant of the bolometer, $\tau = C/G$. The incoming radiation is chopped because the read-out system usually measures the change in the resistance of the bolometer. If one doesn't chop the incoming radiation, the bolometer settles to a new and higher temperature, and the resistance does not change over time under constant radiation.

Therefore, one needs to chop the incoming light to let the bolometer cool down to the original operating temperature, thus creating a constant oscillation in resistance. The time constant **(τ)** of bolometer has to be taking into account due to the heat up and cool down time (Vincent 1989).

Heat conductance **(G),** heat capacitance **(C)** and time constant **(τ)** are the key parameters in the performance characterization of bolometers and they are explained in the following sections.

2.3. Superconducting Transition Edge Bolometers

2.3.1. Brief History of Superconductivity

Many metals and metal alloys undergo a phase transition from the normal state to superconducting state when their temperature decreases from room temperature to near absolute zero. In the superconducting state, the material shows unresistive behavior. In addition, the phase transition occurs at the specific temperature which is called 'critical temperature,' T_c. The critical temperature depends on the composition of materials. The zero resistance behavior was discovered by Kammerlingh Onnes in 1911 and is called 'superconductivity.'

After some years, Walther Meissner and Robert Ochsenfeld discovered that the superconductors exclude magnetic field from their interior. If magnetic field is present in the bulk of the material as it becomes superconducting, the magnetic field is expelled. This is another important property of superconductivity and known today as ` Meissner Effect` (Meissner and Ochsenfeld 1933).

In actuality, magnetic field is not completely expelled from the superconductors. It exponentially decays from the surface of the superconductor inwards. Moreover, some superconductors allow magnetic field lines to penetrate through their bulk. This behavior is explained phenomenologically by Ginzburg-Landau theory (Ginzburg and Landau 1950). The theory examined macroscopic properties of superconductors based on thermodynamic rules. Alexei Abrikosov furthered the Ginzburg-Landau theory, adding that the field penetrates superconductors as quantized tubes of flux which are known as "Abrikosov vortices" (Abrikosov 1957). In the light of this new outlook, he

separated superconductors into two groups based on Ginzburg-Landau theory[1], one of which is dubbed type I where magnetic field decays from the surface and the other is type II, in which the magnetic field can penetrate into the bulk of the superconductor. Although the behavior of type I superconductors was explained by BCS theory in 1957 (Barden, et al. 1957), there is no all-encompassing microscopic theory for type II superconductors.

Generally, low temperature superconductors fall into the type I category and high temperature superconductors fall into type II category. YBCO, which will be the superconducting element in the TEB devices studied in this thesis, is a type II superconductor (Wu, et al. 1987). The history of the development of the field of superconductivity can be found elsewhere (Tinkham 1996, Keterson and Song 1999).

At the present time, the research on superconductors is going on for various applications, both in large and small scale. One of the small scale applications is detectors. Detectors play an important role in the field of experimental science. The detector performance, such as energy resolution and detection threshold, depends very much on the quality of the components that make up the detector. In the case of superconducting transition edge bolometers, responsivity, detectivity and noise equivalent power (NEP) become important parameters for the performance of the detector. In order to study detector fabrication, some important parameters have to be known, especially physical and thermal properties.

2.3.2. Structure of Superconducting $YBa_2Cu_3O_{7-\delta}$ (YBCO)

Long after the discovery of superconductivity, Alex Müller and Georg Bednorz created a new type of superconductor, within a ceramic compound and critical temperature above the liquid helium temperature, called "High Temperature Superconductor" (Müller and Bednorz 1987). In 1987, M.K. Wu and his co workers (Wu, et al. 1987) found another high temperature superconductor called YBCO which it has T_c~92 K, which was above liquid nitrogen temperature and therefore much, much easier to integrate into everyday applications. Partly due to this facilitation, YBCO has been extensively studied worldwide. Since the discovery of YBCO, a lot of research

[1] If $\kappa < 1/\sqrt{2}$ Type I and If $\kappa > 1/\sqrt{2}$ Type II, where κ is the Ginzburg-Landau parameter.

was carried out in large and small scale application areas integrating YBCO, such as power cables and electronic devices. The small scale applications, such as device physics, usually require thin film technologies. As a requirement for these technologies, some structural and physical properties also need to be studied. For example, in the case of transition edge bolometers, the dR/dT value, which depends on the transition temperature, which in turn depends on oxygen stochiometry effects and YBCO crystal structure, is an important parameter to which the responsivity is directly proportional. It is therefore useful to briefly present the crystal structure of YBCO at this point.

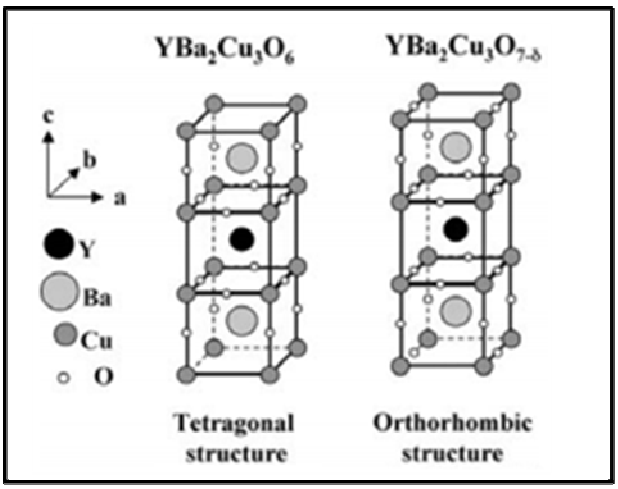

Figure 2. 3. Crystal structure of $YBa_2Cu_3O_{7-\delta}$

(Source: Ayache 2005)

The crystal structure of high temperature superconductors is more complex than elemental superconductors. Most high temperature superconductors have metal oxide (usually copper oxide) layers, causing high anisotropy and complexity compared to pure metal or metal alloy superconductors. $YBa_2Cu_3O_{7-\delta}$, which will be the superconducting material relevant to this thesis, has two copper oxide layers separated by yttrium atom and barium atoms placed at the top and bottom of said layers like a layered sandwich as shown in the perovskite unit cell in figure 2.3. In the copper-oxide planes, copper atoms form a network and oxygen atoms are placed along the copper-oxygen chains as shown in the figure. The superconducting properties of ceramic superconductors mostly depend on the Cu-O planes. Two dimensional CuO_2 sheets are at the electronic hearts of the copper oxide ceramic superconductors. (Izumi and Takayama-Muromachi 1995, Anderson 1997).

Although the crystalline property is not lost when the oxygen content is changed, crystal structure can be changed when oxygen content reaches some certain value. If δ=0.5, $YBa_2Cu_3O_{7-\delta}$ becomes tetragonal and the lattice parameters are a=b=0.387nm and c=1.172nm. If δ=0.1, it becomes orthorhombic and lattice parameters are a=0.382nm, b=0.388nm and c=1.168nm (see figure 2.3) (Mischke 2003). Moreover, $YBa_2Cu_3O_{7-\delta}$ becomes an insulator when δ=1 and structure remains tetragonal. The lowest oxygen value for which the compound is a superconductor is when δ is between 0.4 and 0.3 where it has the lowest T_c (~60K) value for atmospheric pressure and no magnetic field. In contrast, the highest T_c at 92K is achieved with δ=0.3 (Ayache 2006).

2.3.3. Substrate requirements

We purchased YBCO thin films from Theva GmbH commercial company in Germany. They were grown on a variety of substrates (MgO, $LaAlO_3$, $SrTiO_3$) by thermal co-evaporation technique. For growth of high temperature superconductors, R. Wördenweber discusses some basic requirements for good thin film growth for high-T_c superconducting thin films, such as crystallographic lattice match between substrates and HTS films, the mismatch between thermal expansivities of HTS and substrates and chemical inertness of the HTS film with respect to the substrate (Wördenweber 1999). Some common substrates for YBCO that have been widely used are MgO, $LaAlO_3$, yttria-stabilized zirconia (YSZ) and $SrTiO_3$. In this thesis, we have used three different substrates, namely MgO, $LaAlO_3$ and $SrTiO_3$. In order to avoid crystalline mismatch between substrate and YBCO, buffer layer is commonly used in the interface. In our case, 40 nm CeO buffer layer was used in the interface of $LaAlO_3$ and $SrTiO_3$. Due to the importance of sharp transition between normal and superconducting state in the TEBs, the films have to be epitaxial. The result of XRD measurements confirmed that our films have epitaxial, c-axis oriented. Further details will be discussed in detail in the discussion part of this thesis.

In the case of transition edge bolometers (TEBs) some thermal and optical properties of substrates are crucial important such as thermal conductance (G), heat capacity (C), absorption, reflectance and. These properties are summarized in the table 2.2.

Table 2. 2. Thermal and optical properties of YBCO substrates

Substrate Property	**MgO**	**LaAlO**	**SrTiO**
Thickness (mm)	0.5	0.5	0.5
Thermal Conductivity (W/cmK)	<10**[2]	0.32*[1]	$3*10^{-3\dagger}$ [3]
Heat Capacity (J/Kcm^3)	$0.53^{\ddagger}$[4]	$0.59^{\ddagger}$ [4]	0.43[4]
Absoption @ 850nm (%)§ [5]	7.5	22.5	10
Reflectance @ 850nm (%)§ [5]	3	8.5	20
Transmission @ 850nm (%)§ [5]	89.5	69	70

* Nahum and Richards 1991, ** Slack 1962, † Fardmanesh et al. 1995, ‡ Fardmanesh et al. 1999, §Bozbey 2003

The thickness of the substrate has the greatest effect on the responsivity and speed of TEBs (Fardmanesh 1993). Although thick substrates have high optical responsivity, they have relatively slow response due to having large heat storage capacity (C), they take a long time for get rid of heat (Brasunas 1989). In other words, the time constant for thick substrates becomes large. This is undesirable for TEB applications. Thermal conductance (G) also affects the optical response and speed of detectors. Higher thermal conductance can cause small responsivity with fast response and vice versa. Due to the presence of a wide variety of application areas for TEBs such as medical, laboratory and astronomical applizations, which have very different requirements as to the speed and responsivity of the device, C and G are important design factors for bolometers, (Richards, et al. 1989).

2.3.4. Thermal Conductance (*G*)

Wiedemann-Franz law explains the behavior of thermal conductivity for normal metals. The crucial point of this law is the relation between thermal conductance and electrical conductance as (Kittel 1976);

$$\kappa = LT\sigma \quad \text{and} \quad \kappa = \kappa_e + \kappa_l \tag{2.1}$$

where $\kappa, \kappa_e, \kappa_l, L, T$ and σ are the thermal conductivity, the electronic contribution of thermal conductivity, the lattice vibration component of thermal conductivity, Lorentz constant, temperature and electrical conductivity respectively. As

it can be clearly seen in the equation above, thermal conductivity of metals is linearly proportional to the electrical conductivity. In other words, thermal transfer in metals is mostly carried by free electrons rather than lattice vibrations (phonons), even at the low temperatures. In the absence of free electrons in insulators, phonons are responsible for thermal conductance.

However, Wiedemann-Franz law is not completely valid for superconductors. As Cooper pairs cannot transport energy due to being in the ground state at $T < T_c$, the electronic component of thermal conductivity, κ_e, goes to zero. In the case of $T > T_c$, the law is valid because there are no Cooper pairs. Nevertheless, when the temperature of superconductor is close to $T_{c\text{-onset}}$, the behavior remains the same as normal metals because of large amount of quasi-particles (Kadin 1999).

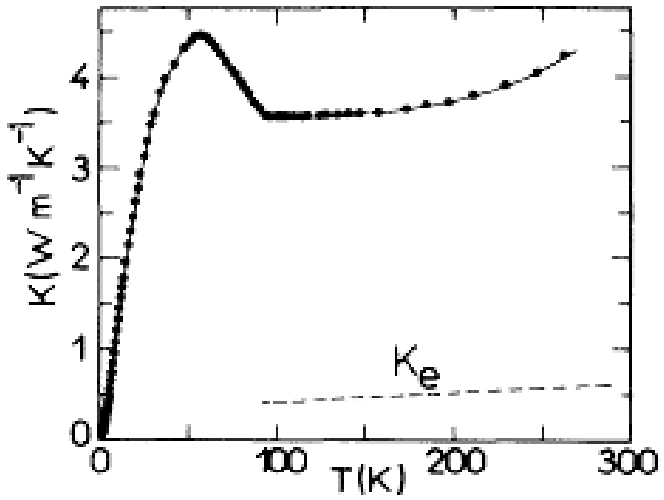

Figure 2.4. Behavior thermal conductivity of YBCO as a function of temperature (Source: Uher and Caiser 1987)

The thermal conductivity determination of superconducting YBCO was performed by C Uher in 1987 for the first time (Uher and Caiser 1987). He carried out the thermal conductivity as a function of temperature as shown in figure 2.4. Still, the electronic component of thermal conductivity in the metal normally decreases when temperature decreases, as it can be clearly seen in the figure. The thermal conductivity of YBCO increases at the transition region; this is the evidence of increasing scattering between phonons and quasi-particles. Due to the anomaly of the temperature range in the figure 2.4, most of thermal transport is carried by phonons rather than the electronic component. In the temperatures below T_c, phonon contribution becomes dominant and

quasi-particles are frozen out and they cannot contribute to the thermal transport at all. In the case of transition edge bolometers (TEBs), phonons are responsible to the thermal conductivity because TEBs are operated at the middle of transition region with fixed temperature. However, the thermal conductance between substrate and thin film interface is also important and it is resistive to heat conduction, generally known as "Kapitza Resistance." It can be noted that in our case the thermal conductance between film and substrate is not important because of working at the low frequency regime and it will be explained in detailed in the next parts (Fardmanesh 1995). The measurement of thermal conductance in the interface between film and the substrate can be found elsewhere (Robbes et al. 1999, Prasher and Phelan 1997). We have measured the total thermal conductance of the system by the "Joule heating" method which will be explained in the experimental part.

2.3.5. Heat Capacity (*C*)

Heat capacity or specific heat (heat capacity per unit volume) has two components, which are electronic specific heat capacity, C_e, and lattice vibration (phonon) contribution to the heat capacity, C_{ph}. At high temperatures and near room temperature, only 1% of electronic heat capacity can contribute to the overall specific heat. On the other hand, almost all the specific heat is carried by phonons. According to the Debye approximation for metals (Kittel 1976), the phonon specific heat, C_{ph} decreases with temperature and at in the sufficiently low temperature region it decreases with T^3. In contrast, the electronic specific heat, C_e decreases linearly with temperature, $C_e \sim T$, as shown in the figure 2.5. When the temperature approaches to zero, no anomaly in the behavior of both electronic and phononic specific heat can be seen.

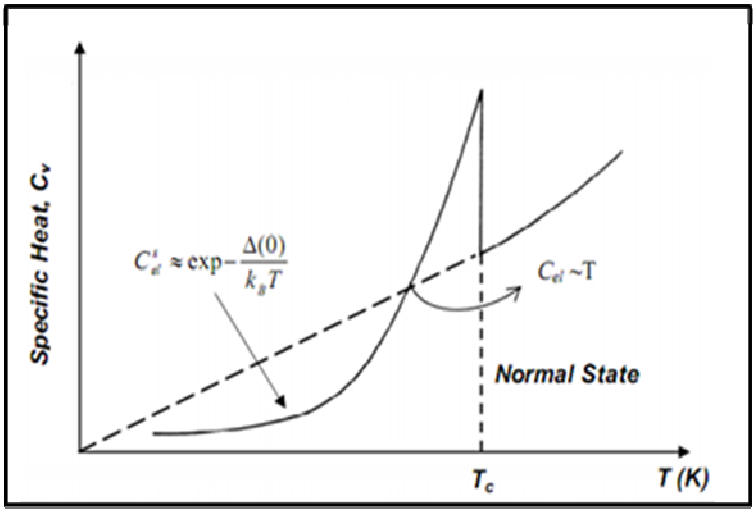

Figure 2.5. Behavior specific heat of superconductors as a function of temperature (Source: Omar 1993)

The specific heat behavior of superconductors is different from the metals. It can be clearly seen in figure 2.5 that there is a specific jump in the transition region. At the superconducting region the electronic specific heat decreases exponentially, $C_e \approx \exp(-\Delta(0)/k_B T)$, while the phononic behavior remains the same as the normal metals. This jumping behavior can be explained with the BCS theory which dictates that there is an energy gap between normal and superconducting region. The electrons can form Cooper pairs at the ground state. In addition, the Cooper pairs cannot store any form of energy. Moreover, quasiparticle density largely decreases below the transition temperature. Near T_c, the quasiparticles start to form cooper pairs. This means the electrons move from excited to the ground state. As a result, this jump is the clear evidence of energy gap in the transition region. Although specific heat behavior of type I and type II superconductors have some differences, the approximation of BCS theory remains the same (Werner 1991, Williams 1993, Loram et al. 1993).

2.3.6. Time Constant (τ)

The basic working principle of transition edge bolometer is based on thermally heating up and cooling down process as previously described. When the incoming radiation strikes the YBCO thin film absorber, the temperature of YBCO is increases

and when it is chopped, the temperature decreases to the heat bath temperature as shown in figure 2.6. The time taken for the temperature to change by *1/e* of the maximum change is called the "time constant (τ)," and it is expressed by $\tau = C/G$ (Duzer 1999, Tseng 1991, Lambkin 1999).

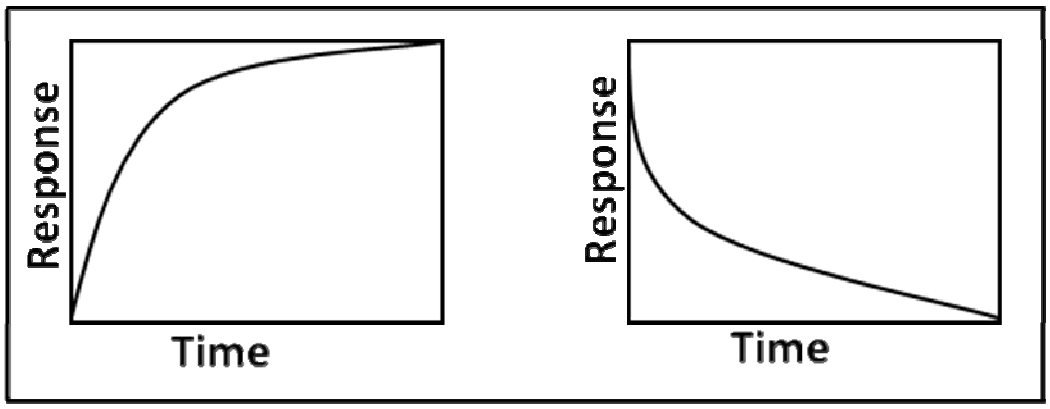

Figure 2. 6. Schematic of heat up and cool down time of bolometer

Time constant of a bolometer depends on its overall heat conductance (G) and heat capacitance (C). In order to make a TEB with fast response, the heat capacitance has to be decreased or thermal conductance has to be increased. For this purpose, membrane or micromachining technology is widely used (Li et al. 1993, Yoon et al. 1999, Mechin et al. 1996, de Nivelle et al. 1997, Lakew et al. 2004). However some research groups reported that the speed of high temperature bolometers can also be improved with constant voltage bias (to the order of μs), but in this case SQUID readout is required (Irwin 1995, Lee et al. 1998). The other solution suggested by Qing Hu (Hu and Richards 1989) utilizing antenna-coupled microbolometers. They reported that the responsivity can be increased without decreasing the speed of response when antena-coupled to a bolometer but complex design is required for this purpose.

The time constant of our bolometer, as measured by oscilloscope, is on the order of milliseconds without using any special design (the thickness of our substrate is 0.5 mm).

2.4. Figures of Merit for the Transition Edge Bolometer

The goal of this work is mostly focused on the investigation of basic figures of merit for transition edge bolometers. In order to characterize and quantify the performance of transition edge bolometers, we used some common figures of merit which are optical voltage responsivity, R_v, noise equivalent power *(NEP)* and detectivity, D^*. All of these parameters are interrelated. They also depend on some parameters such as thermal conductance (G), heat capacitance (C) and time constant (τ). Although these parameters enable us to compare the relative detector performance, just one of figure of merit cannot completely characterize bolometer performance, except perhaps for detectivity. However, in order to calculate detectivity of bolometer optical responsivity and noise equivalent power have to be known.

2.4.1. Optical Responsivity

The responsivity of bolometers can be classified into two groups, which are bolometric (equilibrium or thermal) and non-bolometric (or non-equilibrium) response. The mechanism of non-equilibrium response is more complicated than bolometric response. Nevertheless, non-bolometric response is observed at the superconducting state or well below T_c while bolometric response is observed both at the T_c and above. The non-bolometric response is observed more often in the junction based bolometers such as grain boundary weak link Josephson junctions in the granular thin films (Hao et al. 1993, Frankel 1993) and the response time is much faster than bolometric response which in the range of ns and ps. At the same time they have higher intrinsic noise than epitaxial films because the flux flow through the superconductor is responsible for high noise. In this thesis we have investigated the bolometric response in the highly c-axis oriented YBCO thin films.

Due to low infrared absorption of YBCO (~10%) sometimes additional absorption layer is coated on the surface of the bolometers. Such bolometers are called “composite bolometers” (Clarke et al. 1977, Ivanov et al. 2007, Moftakharzadeh et al. 2008). This type bolometers have both high responsivity and low noise value. The

bolometer without an absorption layer is called “monolithic bolometer” which is the type used in this thesis.

RC Model

In order to model the responsivity of TEBs, the analogy between electrical circuit and thermal circuit can be considered as in table 2.3. (Bozbey, 2003)

Table 2. 3. The analogy between electrical circuit and thermal circuit

Thermal Parameter	**Electrical Analog**
Heat flow (Watt)	Current (Ampere)
Temperature (Kelvin)	Voltage (Volt)
Thermal Conductance (Watt/Kelvin)	Conductance (1/Ohm)
Heat Capacitiy (Joule/Kelvin)	Capacitance (Farad)

As we mentioned at the beginning of the chapter, the basic function of a bolometer is to convert input radiation power to electrical output signal such as voltage or current depending on bias type. In our case, we biased our bolometers with a constant current and obtained a voltage response R_v. As shown in figure 2.2, the radiation is modulated with an angular frequency ω, and power, P_0, through the heat sensitive element and substrate having heat capacity C, which are thermally linked, G, to the heat bath in a constant temperature,T_0. The resistance of absorbing element is changed due to the rising temperature, T, by the incoming radiation and it is given by:

$$\Delta R = \frac{\alpha R \eta P_0}{(G^2 + \omega^2 C^2)^{1/2}} \tag{2.2}$$

where η is the absorption coefficient of thin film and α is the temperature coefficient of resistance (TCR) which is always positive for superconductors and negative for semiconducting materials (Richards 1994). It is given by $\alpha = \frac{1}{R}\frac{dR}{dT}$. In order to prevent thermal runaway of the bolometer, the current must be limited with

(Verghese, et al. 1991) $I^2R \leq G/\alpha$,. We have operated our devices with this consideration.

For a given current bias level I_b, the voltage signal V_s is,

$$V_s = \frac{I_b \alpha R \eta P_0}{(G^2 + \omega^2 C^2)^{1/2}} \tag{2.3}$$

where τ is the time constant $\tau = C/G$. The optical voltage responsivity is given by the signal voltage per incident radiation power and has the units of [V/W] (Richards 1994, Kruse 1990):

$$R_v = \frac{V_s}{P_0} = \frac{I_b \alpha R \eta}{G(1 + \omega^2 \tau^2)^{1/2}} \tag{2.4}$$

The RC model can explain well the optical voltage responsivity of TEBs at low chopping frequency regions. However at very high frequencies, some advanced models have to be taken into account and can be found in literature (Bozbey 2003, Fardmanesh 1995).

2.4.2. Noise Properties of Transition Edge Bolometers

Noise is the undesirable electrical signal output which contributes to the desired electrical signal from various sources. It is not possible to eliminate noise from the system entirely, nor is it easy to measure and quantify noise. In addition, noise is a random fluctuation of electrical signals at the vicinity of average measured signal. Most of time noise appears at specific frequencies such as mechanical vibrations, acoustic vibrations, temperature fluctuations, microwaves or radio waves coming from environment even due to working frequency of the measurement electronics. Although elimination of environment noise sources is relatively easy, there is no possibility to get rid of noise in the material because some of it depends on crystal structure and device fabrication quality, while others such as Johnson noise is a fundamental phenomenon. Some known sources and mechanisms of noise is widely investigated both

experimentally and theoretically (Khrebtov 2002, Richards 1994, Szentpali 2007, Fardmanesh et al. 1996, Verghese et al. 1991, Kraus 1996). Some of intrinsic noise sources are thermal (phonon) noise, photon noise, amplifier noise, Johnson noise and 1/f noise.

Thermal noise is known as phonon noise. The random exchange of energy carriers between absorber element of bolometer and heat bath through weak resistance (thermal resistance). Due to instabilities of temperature, phonons and quasi-particles which are energy carriers can collide with each other while they move from absorber to heat bath and with the result of this collision the resistance can change randomly. Most of this noise is due to the phonons moving through the thermal boundary between two materials. In order to minimize temperature fluctuations, large heat bath with a large heat capacity can be used.

Photon Noise: According to Stefan-Boltzmann law, all objects can radiate photons at any nonzero temperature. Energetic photons that are randomly exchanged between environment and detector cause photon noise. In order to reduce of this type of noise the detector needs to be shielded from environment and must be kept sufficiently cold, but it is impossible to completely eliminate this noise.

Johnson Noise can be seen in all resistors. The random scattering of electrons from the core ions or imperfections in the crystal causes Johnson noise as they are moving in the direction of the current. Johnson noise is the dominant source of noise in thermal detectors and they are seen directly in response voltage.

1/f Noise strongly depends on material used for the detector. Epitaxial growth of high temperature superconductors can reduce the 1/f noise by eliminating boundary resistance at the interface with buffer layer. In addition to the structure of thin films, the operating frequency also affects this type of noise, because it is inversely proportional to the frequency.

Amplifier Noise can be removed by appropriate impedance matching between detector and measurement electronics especially the lock-in amplifier.

In order to mention the sensitivity of a bolometer, the “noise equivalent power (NEP)” has to be take into account. It is impossible to talk about bolometer sensitivity without NEP. NEP is the amount of input power that would give an SNR of 1 in a unit frequency bandwidth. NEP is given by dividing noise voltage to the responsivity,

$$NEP^2 = \frac{VoltageNoise}{\mathrm{Re}\,sponsivity} = \frac{4k_B T^2 G}{\varepsilon^2} + \frac{4k_B T^2 R}{|R_v|^2} + \frac{8\delta k_B A T_B^2}{\varepsilon} + \frac{V_{1/f}^2}{|R_v|^2} \qquad (2.5)$$

The equation (2.5) includes phonon noise, Johnson noise, photon noise and 1/f noise respectively (Khrebtov 2002, Moftakharzadeh et al. 2008). As we mentioned above, the dominant terms are phonon and Johnson noise and the other noise sources can be neglected.

One of the advantages of superconducting YBCO transition edge bolometers is having relatively small NEP. The smallest (best) NEP was reported which is $\sim 4.5x10^{-12} W/\sqrt{Hz}$ at 10 kHz, for monolithic and antenna-coupled bolometers (Nahum, et al. 1991).

We have measured noise with a lock-in amplifier, therefore obtaining the overall noise as opposed to a noise spectrum as it will be explain in the experimental and discussion part.

2.4.3. Detectivity (D^*)

As detectors of different sizes will have different NEPs, The size of the detectors should be taken into consideration when calculating NEP. The detectivity, D^*, can give us complete performance about sensitivity without any other parameter and it is defined as;

$$D^* = \frac{\sqrt{A_d}}{NEP} = \frac{\sqrt{A_d \Delta f}\, R_v}{V_n} \qquad (2.6)$$

The equation (2.6) includes effective radiation absorption area ($\boldsymbol{A_d}$) of the bolometer, operation frequency bandwidth ($\boldsymbol{\Delta f}$) and the responsivity due to the knowledge of NEP. The highest detectivity for high temperature superconducting YBCO bolometers has been reported at about $3x10^{10} cm\sqrt{Hz}/Watt$ for 10μm wavelength (Verghese, et al. 1992).

CHAPTER 3

EXPERIMENTAL DETAILS

This chapter consists of two main parts. In the first part, patterning procedure of the devices is detailed, including mask design, photolithographic process, etching and gold deposition (contact metallization). The second part of this chapter is about characterization of patterned devices, including electrical and bolometric measurements.

3.1. Device Patterning

In the device fabrication technology the most important process is patterning. The patterning process affects the performance of devices in all characterization steps. In order to fabricate high quality devices, patterning techniques have been investigated for many years and it is still an ongoing research area. At the present time, many advanced patterning tools are available such as ion milling, focused ion beam (FIB) and electron beam lithography. After developing very high resolution lithographic techniques, devices have become smaller and smaller as in the novel nanoelectronics research branch..Photolithography is the oldest technique and it works well for down to 0.5 μm device patterning.

In this thesis we have used three YBCO thin films grown on different substrates, namely magnesium oxide (MgO), lanthanum aluminate ($LaAlO_3$) and strontium titanate ($SrTiO_3$). The film thickness on the MgO is 300 nm and the film has no buffer layer. On $LaAlO_3$ and $SrTiO_3$, the film thickness is 200 nm with 40 nm cesium oxide (CeO) buffer layer at the interface of the film and substrate. We have patterned each thin film with four different width and area configurations except $SrTiO_3$ which is patterned for four identical (with same width and area) devices. The physical properties of patterned devices are summarized in the table 3.1. In order to pattern the devices, we first designed two types of masks for positive and negative photolithography. After that, the

devices were chemically etched and finally gold deposition was performed in order to make electrical contacts.

3.1.1. Mask Design

The mask design is the first process of device patterning. The resolution of masks has to be very high for submicron patterning applications. However, in our case, this is not as crucial because the lowest dimension of device is 30 µm. We have designed several meander and micro-bridge mask sets for the patterns and contact layers, each set implemented twice for positive and negative photolithography. Positive type masks were utilized for photolithography and etching process while the negative masks were used for gold deposition process. We have four different type devices on each chip having meander shape. The widths and area of devices include large-small areas, with thin and thick widths (see table 3.1 for details). For this purpose, we have designed the masks using CorelDraw^{TM} graphic software and obtained printouts on acetate with a 3000 dpi printer. The details of drawn masks are shown in figure 3.1.

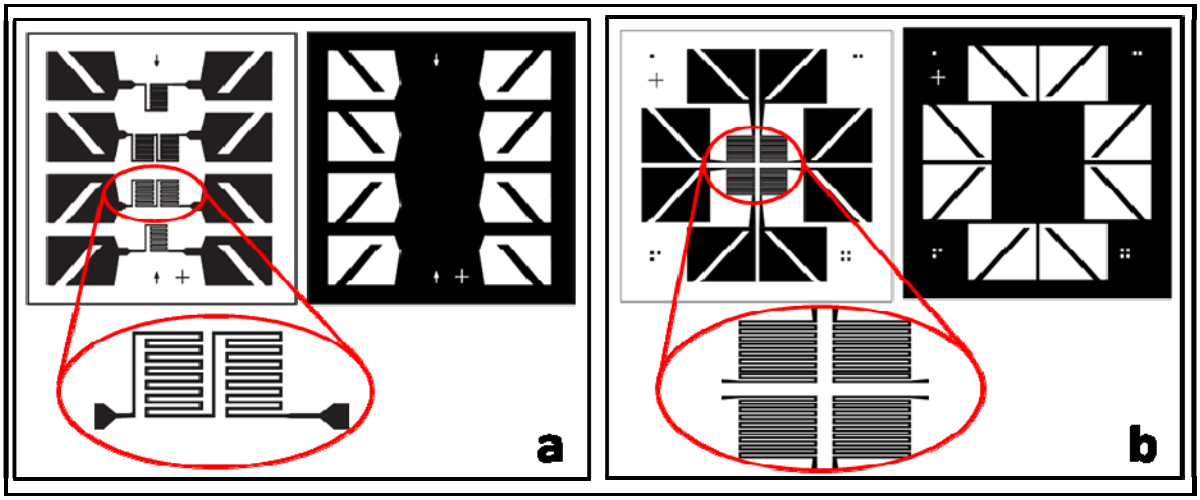

Figure 3.1. The positive (left), negative (right) masks and the detail of meander for a) MgO (B_1), $LaAlO_3$ (B_2) and b) meanders for $SrTiO_3$ (B_3) chips

3.1.2. Photolithography Process

Photolithography is a process used to create a pattern on a surface of thin film for device applications. The standard process of photolithography consists of photoresist coating, soft baking, UV exposure, development and hard baking. Each of these steps is described in detail below.

The first step of photolithography is photoresist coating and it requires very clean surfaces in order to achieve a uniform coating. The surface of YBCO thin films were cleaned by acetone and isopropyl alcohol (C_3H_8O) and dried with nitrogen gas. Cleanness was checked under optical microscope. The process was repeated until satisfactory results were obtained. This was one of the most important steps for patterning because if film surface contains some dust before coating, the photoresist cannot be uniformly distributed and hillocks appear on the dusty region. This causes a deformation of patterns after the development process.

After the cleaning process was completed, the film was glued to the center of spinner by bilateral tape and three droplets of photoresist (positive, AZ1505) put on the surface of film by an unused pipette and after the second droplet, the spinner was turned on for 1min. For this purpose we used homemade spinner as shown in the figure 3.2a.

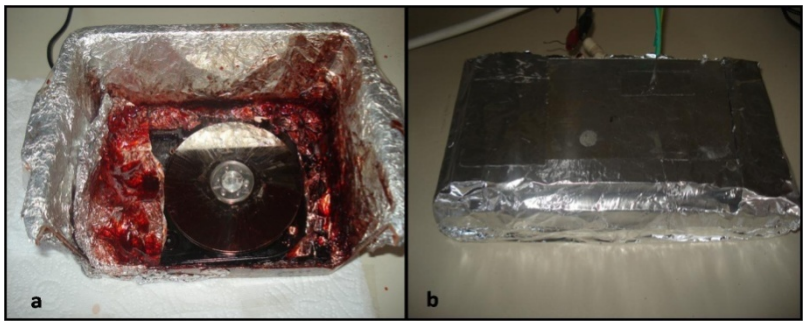

Figure 3.2. a) Spin coater made with computer hard disc (5400 rpm), mounted on the vessel shielded from environment by aluminum foil. One side of vessel is cut in order to take film off on the spinner easily. b) Hot plate made with two aluminum plates.

We used 5400 rpm hard disc for coating of surface with photoresist. This is a very good and cheap alternative to commercial spinners as old hard disks are easy to come by and there is no wobble when they spin.

After coating surface with photoresist, we baked the film at 100 ^{0}C for 75 seconds in the process called “soft bake” over a homemade hot plate as shown in figure 3.2b. This process makes the photoresist sensitive to ultraviolet (UV) light. Note that the temperature has to be uniformly distributed on the surface. The temperature gradients on the surface of film would lead to irregular development of the photoresist (positive, AZ1505) in the later stages.

The soft-bake step was followed by UV exposure. We aligned the mask on the surface of coated film by using xyz-stand as shown in the figure 3.3. We made sure that the mask touches the surface of coated film uniformly by visual inspection through an optical microscope. The mask has to be accurately aligned on the surface of coated film without any separation between mask and the surface of film; otherwise UV can penetrate under the mask pattern and cause defects on the pattern of the film after development.

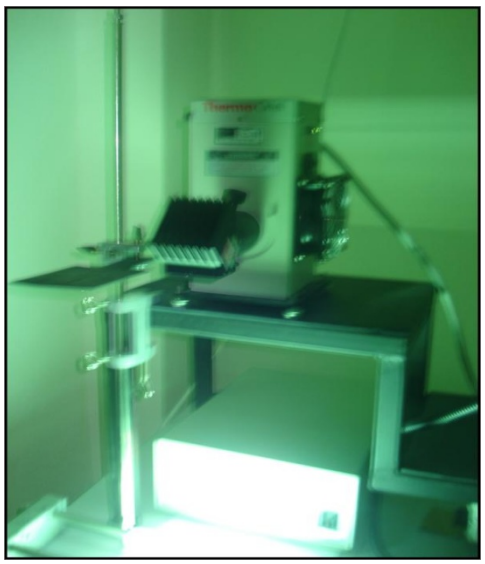

Figure 3.3. UV with 200W power and xyz-stand for alignment.

After mask alignment, we exposed our films to UV light for 22 seconds. After UV exposing, we developed (AZ 726 MIF Developer) the coated film for 5-6 seconds and immediately washed the film with DI water. We observed with naked whether the

film patterned or not, if not the development process had to be repeated until the general pattern of film appeared. After creating the photoresist pattern on the surface of the film, we checked it by optical microscopy. If the pattern was faulty, the photoresist was cleaned with acetone and the whole process was started over.

The photolithography process was completed with hard baking. In order to make photoresist harder, we baked our film at 115 ^{0}C for 65 second. After this process, photoresist behaves like a mask and it protects the film during the etching process. The photolithography process is summarized in figure 3.4.

3.1.3. Etching

Etching process is the last part of the patterning of our films. We used chemical etching, also called "wet-etching", for our films. Generally, the resolution of wet etching is limited to about ~0.5 μm, but in our case, the smallest pattern is 30 μm so wet etching is appropriate for our purpose.

The process is one of the most critical parts of patterning because of its irreversibility. Nevertheless, this process involves some important requirements. In order to etch the film with a good resolution the chemicals have to be as clean as possible, otherwise the etchant will cause under-etching. This means that the acid (etchant) will eat the accumulated dirt under the photoresist and cause the removal of device patterns (etch-away).

For this process we used 0.5ml phosphoric acid (H_3PO_4) in 100ml DI water.as etchant and waited for ~10 seconds in the acid. It is possible to see the reaction of acid and film by naked eye so waiting time can be adjusted as the pattern of device appears. After the film was taken out from the acid, it was immediately put into DI water for ~15 sec. The device pattern was then checked under the optical microscope. If necessary, this procedure can be repeated, but the waiting time in the acid has to be small (around 2-3 seconds).

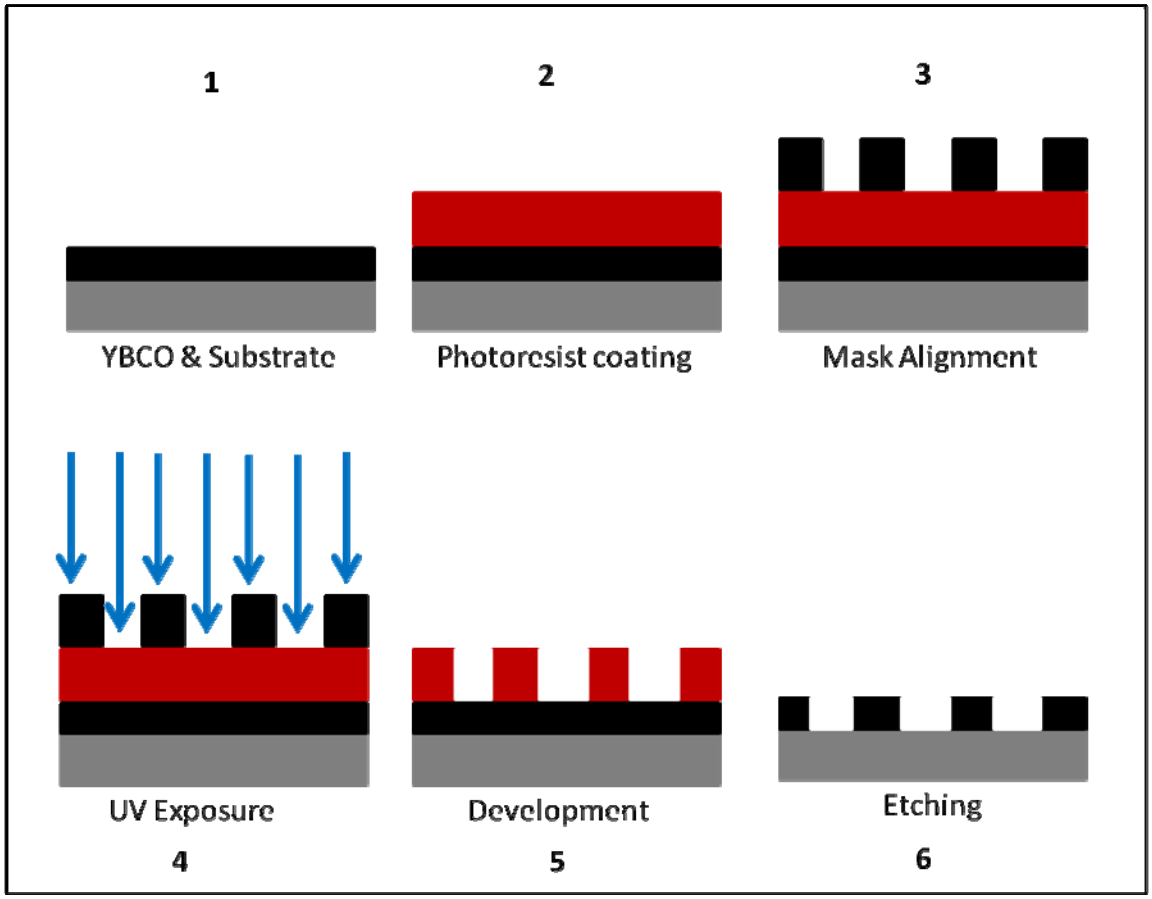

Figure 3.4. Summary of Photolithography and Etching process 1) Cleaning the surface of film, 2) Photoresist coating, 3) Mask alignment by xyz-stage, 4) UV exposure through the mask, 5) Development by developer, 6) The film etched by phosphoric acid

(Source: Avci 2007)

3.1.4. Gold Deposition (Contact Metallization)

After the patterning process, contact pads of the device were deposited by gold in order to assure ohmic behavior between the film and contact wire. Gold deposition is protecting contact pads from oxidation. Otherwise, the oxidized layer can behave like an insulator between the film and the contact. This process also protects the film during contact wiring, otherwise the film can be damaged and good contacts cannot be provided.

Gold deposition was performed by SPI Sputter coater as shown in the figure 3.5 under the following deposition conditions:

- $P_{Ar}=8*10^{-1}$mbar
- I_{DC}=15mA
- Target-Substrate distance = 4cm
- Deposition time = 2.5 min

Figure 3.5. SPI Sputter coater for gold deposition.

We have used lift-off technique in order to remove gold from the contact pattern region. Negative mask was used in the photolithography process as mentioned above. The same procedures were followed for gold contact pattern. After gold deposition on the film surface, gold liftoff was achieved by using an ultrasonic cleaner for 2-3 sec. Finally, the film was cleaned by acetone and alcohol.

After gold deposition, we used silver paint to glue thin copper wires on to the device's contact pads. By this way, ~0.05 Ω contact resistance was achieved in the superconducting state.

Table 3. 2. The code and physical dimensions of patterned devices

Device Code	Width, Area	Substrate*	Film Thickness
B_1M_1	30μm, 0.3 mm^2 (Thin-Small)	MgO	300 nm
B_1M_2	30μm, 0.6 mm^2 (Thin-Large)	MgO	300 nm
B_1M_3	50μm, 0.5 mm^2 (Thick-Small)	MgO	300 nm
B_1M_4	50μm, 1 mm^2 (Thick-Large)	MgO	300 nm
B_2M_2	30μm, 0.6 mm^2 (Thin-Small)	LAO (CeO buffer)**	200 nm
B_2M_4	50μm, 0.5 mm^2 (Thick-Small)	LAO (CeO buffer)**	200 nm
B_3M_2	30 μm, 0.54 mm^2	STO (CeO buffer)**	200 nm
B_3M_3	30 μm, 0.54 mm^2	STO (CeO buffer)**	200 nm

*(10x10x0.5mm, c-axis), **The thickness of CeO buffer layer is 40nm

3.2. Characterization

During this work many, characterization techniques were employed. Fabricated films were structurally characterized by x-ray diffraction (XRD), and scanning electron microscopy (SEM) in order to analyze crystal structure and surface morphology in submicron level. The structural results will be given in the discussion part. We performed electrical and bolometric characterizations such as resistance-temperature (R-T), amplitude of response-temperature (A-T), amplitude of response-chopping frequency (A-F), thermal conductance (G), time constant (τ), noise measurements and finally we performed detectivity calculations of our devices.

3.2.2. Resistance-Temperature Measurements

The electrical resistance versus temperature (R-T) measurement is the basic electrical characterization of superconductors. R-T characterization is crucially important for transition edge bolometers (TEBs), because they are operated at the

middle of superconducting transition region. We have performed many R-T measurements in order to find the exact operating temperature point of TEBs. R-T measurements were performed both with and without radiation. For this purpose, we obtained R-T curves for both when the temperature was increasing and decreasing. Finally R-T measurement setup was optimized in order to get the same result for increasing and decreasing temperature. In order to accurately measure resistance, four point contact method was used for all measurements. In our R-T measurements we have used current bias and measured voltage, and calculated resistance. The R-T measurements were performed by Keithley 2400 sourcemeter for driving current, Keithley 2182 nanovoltmeter for voltage measurement and LakeShore 331 temperature controller, which are connected to control computer by GPIB interface (see figure 3.12).

All measurements were controlled by software coded in LabView™ program. During R-T measurements, we took data with temperature increasing with 0.1K steps per 15sec in order to make the temperature sensor and device at nearly the same temperature. dR/dT-T of the samples was also measured and both R-T and dR/dT-T were screened at the same graphic as shown in the figure 3.6. At the end of R-T measurements we found operation temperature of TEBs which is the peak point of the dR/dT graph.

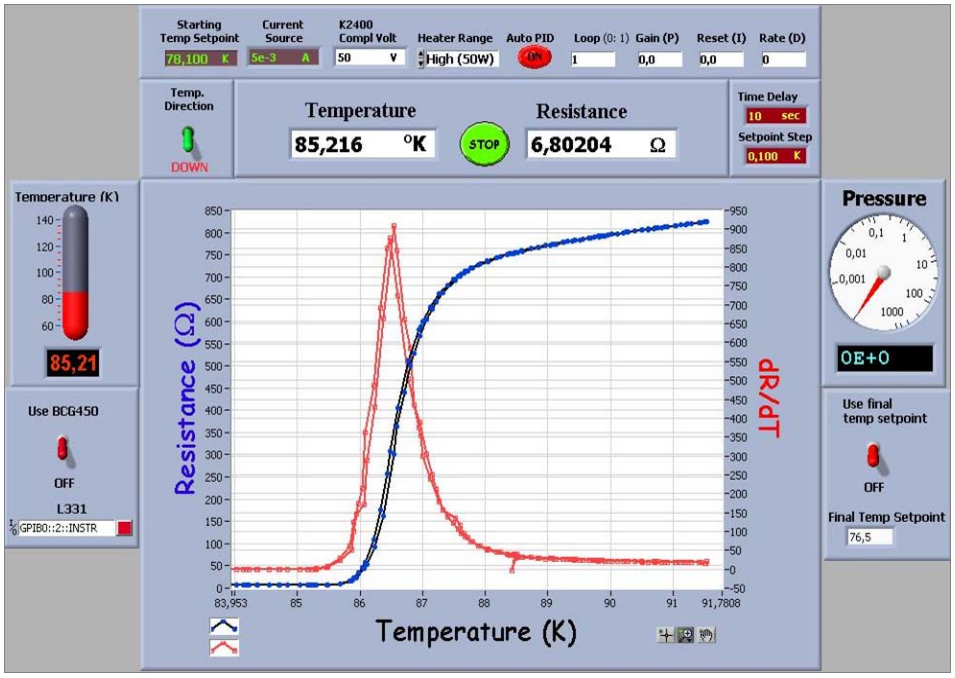

Figure 3.6. R-T and dR/dT-T measurement controlled via LabView™ program.

3.2.3. Temperature – Amplitude of Response Measurements

As it mentioned in the previous section, superconducting transition edge bolometers (TEBs) are operated at the peak point of dR/dT value, because at this point, resistance of the bolometer strongly depends on temperature. We also measure the amplitude of response as a function of temperature. This result gives us the operating point of bolometer as well as dR/dR versusT measurements. As can be expected, the peaks of these data overlap. Another importance of this type of measurement is deciding whether our bolometers' response is bolometric or non-bolometric. All of our measurements indicate a bolometric response because of overlapping dR/dT and amplitude-temperature (A-T) peaks, as will be given in the discussion part.

For this measurement we used Stefan-Boltzmann light source at 3200 K. The radiation was filtered via a highpass infrared (IR) filter which removes radiation under 800 nm. In order to define the wavelength of the radiation after the filter, we used high resolution spectrometer (Ocean Optics, HR2000) and we measured that peak point of our wavelength is 900 nm which is in the near-infrared region. And also we measured the power of radiation by Newport 1830C Optical Power Meter and we got 28.8 μW.

The amplitude of response measurements require lock-in amplifier which measured signal in Voltage unit. The reference signal is our chopping frequency and the lock-in amplifier (SR830) just measures the time varying signal with the same phase and frequency as the reference signal. During A-T measurements, we used Keithley 2400 source meter for current bias. The voltage output from our TEB was connected to the input of low noise preamplifier (Stanford Research System, SR560) in order to get a clearer signal. The output signal from preamplifier was connected to the input of the lock-in amplifier. The lock-in amplifier measured the changing voltage signal created by radiation. The details of measurement setup are shown in figure 3.12. All of the measurement electronics was controlled by LabView^{TM} program via GPIB. One of the measurement runs is shown in the figure 3.7.

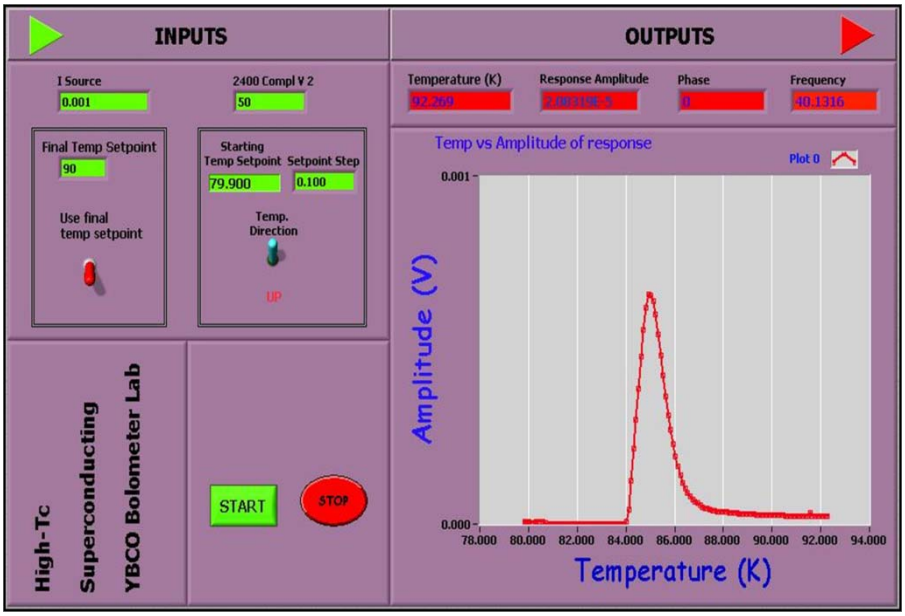

Figure 3.7. LabView™ program for amplitude of response-Temperature measurements.

3.2.4. Frequency-Amplitude of Response Measurements

After finding the exact operating temperature of TEBs from the amplitude-temperature (A-T) and dR/dT peaks, we performed amplitude of response as a function of chopping frequency (A-F) measurements at the constant temperature which was the temperature at the peak point of A-T and dR/dT measurements. Amplitude of response versus chopping frequency is one of the important measurements of this work because in most of responsivity modeling, this measurement has to be taken into account due to including voltage response as a function of chopping frequency. For this measurement we have used Oriel mechanical chopper, lock-in amplifier, low noise preamplifier, Keithley 2400 source meter and Stefan-Boltzmann lamp at 3200K which was passed through the infrared filter. Due to frequency limitation of mechanical chopper, we have used 550 Hz maximum operation frequency.

The temperature stability is crucially important to this measurement because it is impossible to get radiation response signal from detector if temperature fluctuations are high. In other words, temperature fluctuation creates higher voltage signals than resistance which is created by infrared radiation. For this reason, we have achieved $\pm 2mK$ temperature stability as shown in the figure 3.8a. In order to get high temperature stability we have separated liquid nitrogen dewar from cold head by a paper

and six resistors were used as a heater mounted on the cold head as shown in the figure 3.8b.

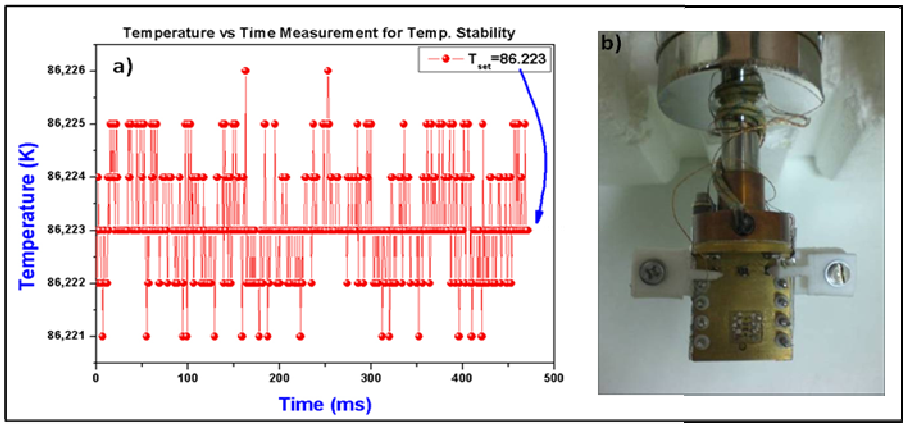

Figure 3.8. ± 2mK temperature stability a) temperature stability measurement result, b) Cold head design

Like other measurements, we have controlled our A-F measurements via LabView™ program as shown in figure 3.9. In this figure both phase of response (red) and amplitude of response (blue) versus chopping frequency are shown. We have only taken into account the amplitude of response in this thesis because the phase of response has an overall additive factor and moreover it is not crucially important for the objective of this work. It can be clearly seen in figure 3.9, there is no temperature fluctuation in the measurement. It can be noted that during all measurements, rough pump was operated. Otherwise, the temperature fluctuations were increased by leakages.

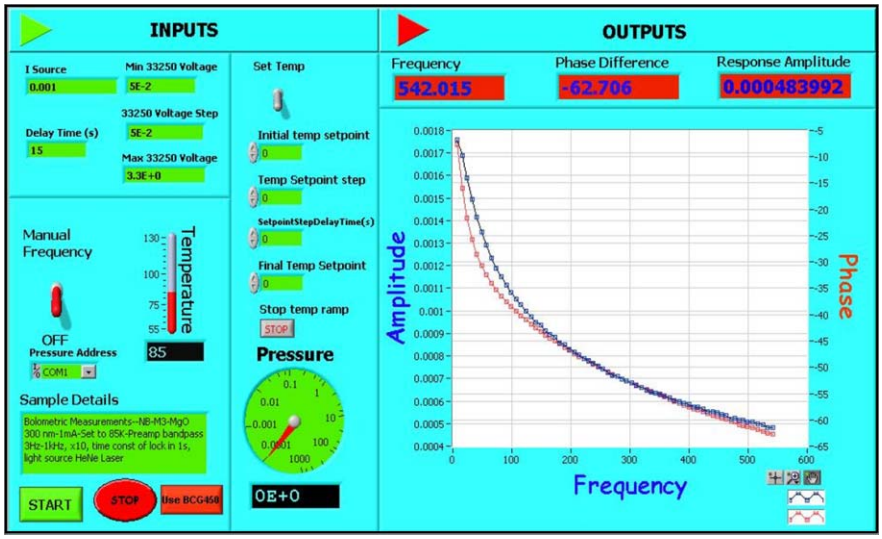

Figure 3.9. Amplitude of response versus chopping frequency measured by LabView™ program

3.2.5. Thermal Conductance and Time Constant Measurements

Thermal conductance is the total heat conductance from the bolometer to its environment per degree of temperature difference. By definition,

$$G = \frac{P_{in}}{\Delta T} \tag{3.1}$$

where ΔT is the temperature difference and P_{in} is the input power that creates the temperature difference. Fardmanesh et al. (Fardmanesh, et al. 1995) reported some techniques for measuring the thermal conductance of bolometers as the key parameter. The "Joule heating" method is one of the most appropriate techniques that measure the thermal conductance of bolometer. In order to realize this method, firstly we measure current versus resistance of YBCO bolometer at a constant temperature just above the superconducting transition region. At that region, thermal conductance of a bolometer is constant as shown in the figure 2.4 and performed by C. Uher (Uher and Caiser 1987). The current-resistance measurement is shown in figure 3.10a and the resistance of the bolometer remains constant until 1.4 mA as the joule heating can be negligible within that region. The bolometer was current biased at different DC currents up to 11mA and

resistance was calculated by dividing measured voltage to the biased current. After that, we carried out the resistance-temperature measurement with a constant bias current, I_b=100 μA, which is in the negligible joule heating region as shown in the figure 3.10b.

After getting the current-resistance (I-R) and the resistance-temperature (R-T) curves, we chose the smallest resistance value, (497.2 Ω) in the I-R graph which is in the negligible joule heating region. We then found the temperature corresponding to the same resistance value in the low bias current R-T graph (92.8 K). We repeated this at a slightly higher resistance value to obtain another set of data (519.6 Ω, 97.3 K). Finally, we calculated the temperature difference between two resistances in the R-T graph and concluded that this temperature difference was created by the joule heating effect of the bias current. In order to calculate thermal conductance we used the definition above as (Bozbey 2003);

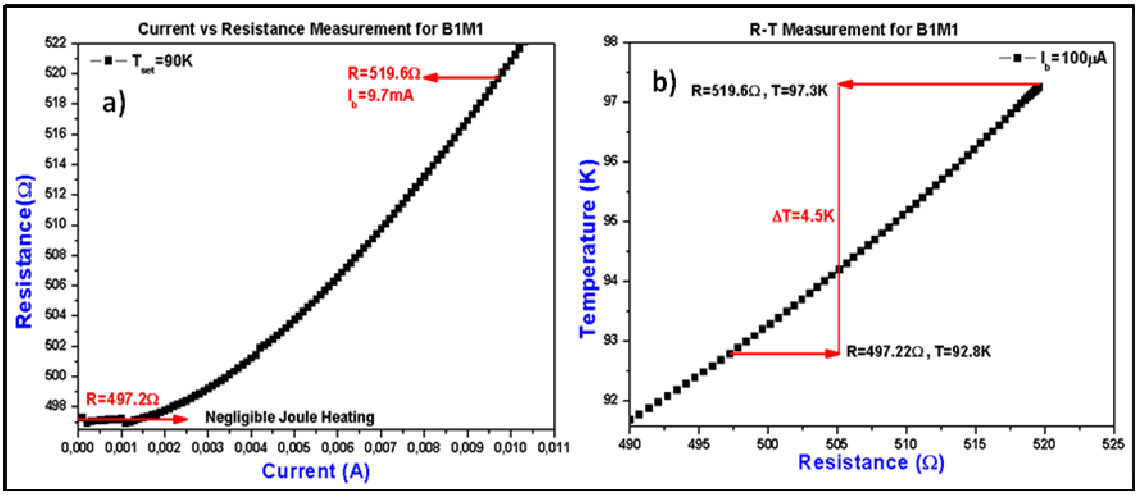

Figure 3.10. In order to measure thermal conductance of devices we used a) Resistance-Current and b) Temperature-Resistance measurements

$$G = \frac{P_{in}}{\Delta T} = \frac{I^2 R}{\Delta T} = \frac{(0.0097A)^2 \times (519.6\Omega)}{(4.5K)} = 11mW/K \qquad (3.2)$$

This value is the total thermal conductance of the whole device system which includes YBCO thin film, the substrate-film and substrate-cold head interface.

Another key parameter of TEBs is the thermal time constant which is defined as the speed of response of the bolometers. In order to measure the thermal time constant

of TEBs, we have used Agilent Tektronix 20 MHz oscilloscope. In this measurement, the TEB was biased with current and the voltage output connected to preamplifier and the output of preamplifier connected to input of oscilloscope. During the measurement, the radiation was chopped with a constant frequency and data was taken from oscilloscope. The time constants of our bolometers are in the order of milliseconds, which is consistent with the values in the literature. An example of time constant measurement is shown in the figure 3.11. Finally we have calculated the whole heat capacitance (C) of our TEBs by $\tau = C / G$.

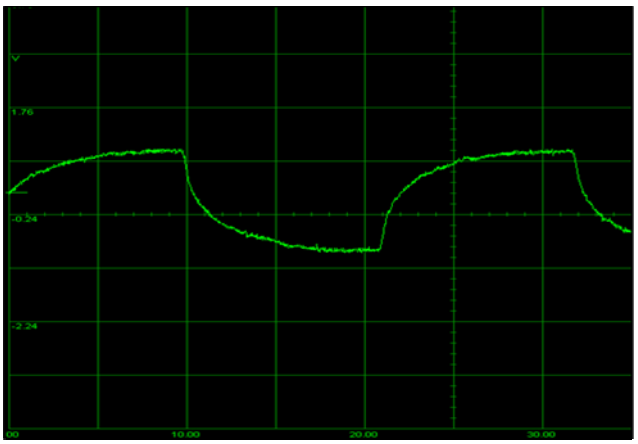

Figure 3.11. The thermal time constant of TEBs measured by oscilloscope

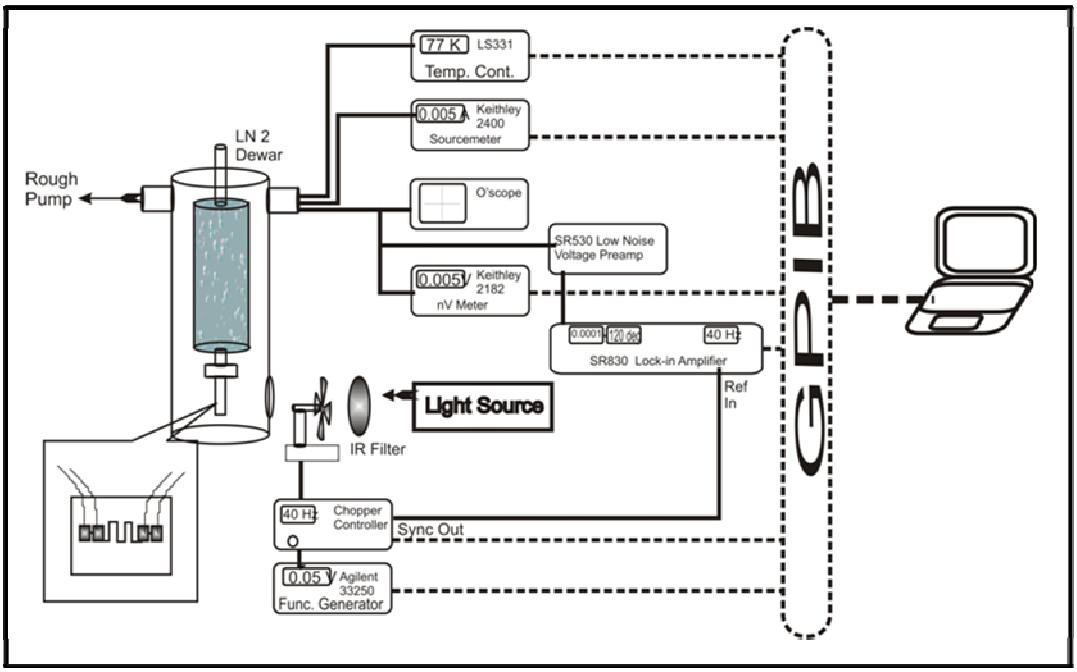

Figure 3.12. The block diagram of electrical characterization setup

3.2.6. Noise Measurements and Detectivity Calculation

In order to measure noise, many things have to be taken into account during the experiment.The device has to be shielded from the environment and it has to be accurately connected to measurement electronics, vibrations from environment has to be isolated. In our measurements we have shielded our system by aluminum folio from environment, all measurements were performed on an optical table and all connections were made by BNC cables, but it is impossible to get rid of noise from the system, especially the intrinsic noises from detector itself which was mentioned in the previous chapter.

After going through the process of minimizing noise, we have measured noise by lock-in amplifier. The measurements results are acceptable when compared to the literature. However, lock-in amplifier measures input signal noise at the input reference frequency. The measured noise signals also at the reference frequency of the lock-in amplifier. In addition noise measurements were carried out at a constant frequency. During measurement light source was illuminated to the detector and the x-noise from lock-in amplifier was obtained.

After noise measurements we calculated the noise equivalent power (NEP) by the basic definition which mentioned in the previous chapter. The experimental part is completed by calculating detectivity. As I mentioned in the 2^{nd} chapter the detectivity gives complete performance knowledge about detector. In order to calculate detectivity both NEP and area of the device has to be known after that detectivity can be easily calculated by dividing area of device with NEP.

CHAPTER 4

RESULTS AND DISCUSSION

This chapter consists of two main parts which are structural analysis and electrical-bolometric characterization. The structural part is divided into two subsections. The first section is x-ray diffraction analysis while the second is scanning electron microscopy (SEM) analysis. The electrical-bolometric characterization part is divided into five subsections which are resistance versus temperature (R-T) measurements, amplitude of response versus temperature (A-T), amplitude of response versus frequency (A-F) measurements, noise measurements and finally calculated detectivity results are given. In each subsection three type chips which are MgO (B_1), $LaAlO_3$ (B_2) and $SrTiO_3$ (B_3) based devices are studied.

4.1. Structural Characterization Results

4.1.1. X-Ray Diffraction (XRD) Characterization

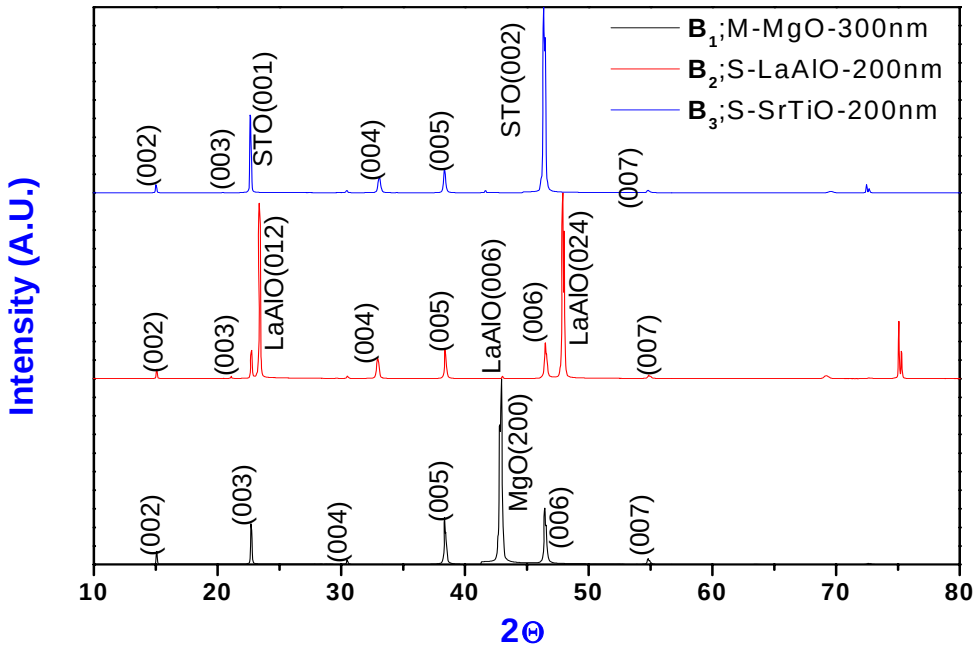

Figure 4.1. XRD results for chip B_1, B_2 and B_3 which are used in this work

The epitaxial growth and characterization of YBCO has received a lot of attention until now and he XRD characterization is one of the common techniques which are used to determine epitaxy and the crystal structure of the thin films. In order to approve the crystalline quality of our films XRD characterization was performed. The x-ray diffraction rocking curve width of (005) peak, which is a measure of crystalline perfection, was measured for our films. The XRD characterization was performed for the three films fabricated on different substrates and the results are given in the figure 4.1. The full width at half maximum (FWHM) of the (005) peak of the films grown on MgO, $LaAlO_3$ and $SrTiO_3$ have 2θ as 0.24^0, 0.26^0 and 0.27^0 respectively, indicating that our YBCO films are highly c-axis oriented.

4.1.2. Scanning Electron Microscopy (SEM) Characterization

SEM is a powerful tool which can characterize the surface morphology of materials in submicron and micrometer scale with a high resolution. In this work, we have characterized the surface morphology of our thin films (B_1, B_2 and B_3) in the 5μm resolution as shown in the figure 4.2. We have purchased two types YBCO thin films having different qualities, one of them called "S" and the other "M" type which are named by growth company. The "M" type films can have a good performance for microelectronics as in our case while the "S" type films have very good quality and fabricated for SQUIDs and micrometer-line width. As it can be seen in the figure the high quality films (S type) have smooth surface which are used for chip B_2 and B_3, while M type films might be seen as rough and used for chip B_1.

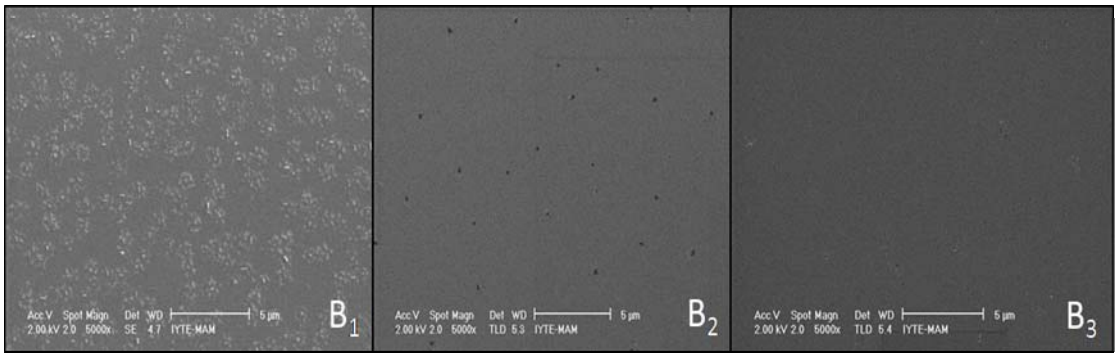

Figure 4.2. Scanning Electron Microscopy (SEM) results for chip B_1 (MgO), B_2 ($LaAlO_3$) and B_3 ($SrTiO_3$) used in this work

4.2. Electrical and Bolometric Characterization Results

This part consists of resistance versus temperature (R-T) measurements and bolometric measurements, which include amplitude of response versus temperature (A-T) and amplitude of response versus chopping frequency (A-F). The detectors were first characterized with R-T measurements with different bias currents in order to find the appropriate operating bias current for avoiding thermal runaway as mentioned in the second chapter. The bolometric characterization was started with A-T measurements with the chosen current from R-T measurements. During A-T measurements, radiation was applied at a constant chopping frequency. Finally, the bolometric measurements were made, obtaining the amplitude of response versus chopping frequency (A-F) data. These measurements were performed at a constant temperature which is the peak point of A-T or the derivative of R-T curve (T_c).

In this chapter, the chips and devices are coded depending on substrate of thin film and the order of devices. B_1, B_2, B_3 will refer to MgO, $LaAlO_3$ and $SrTiO_3$ based thin films respectively and in each chip's devices are coded according to the order of meanders such as B_1M_1, B_1M_2, B_3M_3, B_2M_4 whose first two meanders are thin (in width) and the last two meanders thick (in width). The details of physical properties are shown in the table 4.1, 4.2 and 4.3.

4.2.1. Resistance vs. Temperature Measurement Results

Resistance versus temperature (R-T) measurement is the basic electrical characterization of superconductors. In this work, many R-T measurements were carried out for each device and all measurements were performed under illuminated radiation via a constant chopping frequency such as 40 and 20 Hz. Hence, after the measurement of R-T for different bias currents, appropriate current was found from these measurements in order to provide negligible joule heating effect and hence it was proved by thermal conductance measurement. Consequently, we decided that 2mA operating bias current is acceptable for all devices.

As mentioned in the previous parts, TEBs are operated at the middle of superconducting transition region at the peak point of dR/dT versus T curve. Therefore the R-T measurements have to be accurately performed. In order to accurately measure R-T of the TEBs, the temperature was increased by 0.1K per 15 seconds by a LabView^{TM} program, ensuring the proper thermalization of the system and precise readout.

4.2.1.1. R-T for Chip B_1

The R-T measurement was performed for YBCO grown on MgO substrate. The chip consists of four devices which have different physical dimensions as listed in table 4.1. The normalized R-T measurement for devices patterned on MgO substrate is shown in the figure 4.3 and inset shows un-normalized scale and also the dR/dT versus T measurement for this chip is shown in the figure 4.4. According to these figures, device B_1M_2 has the highest resistance and also the highest dR/dT value which are 606Ω and 926Ω/K respectively. The device B_1M_4 has the lowest resistance (29Ω) and dR/dT (59Ω/K). As can be clearly seen, the large area devices (B_1M_2 and B_1M_3) have higher resistance at the $T_{c\text{-}onset}$ than small area devices (B_1M_1 and B_1M_4) which are one order of magnitude smaller when compared to large area devices. The details of measurements for chip B_1 is shown in the table 4.1. These results are expected because resistance can be increased with the length and decreases when width increases. Although the contact

resistance of the devices are on the order of $10^{-3}\Omega$, this value becomes higher for device B_1M_4 and it is about 10^{-2} Ω. This could be due to the photoresist residue remaining between contact pads and the thin film. Actually this value does not affect the response. Moreover the superconducting transition width of the devices is also important and both the magnitude of response and the speed of response increases when the width of transition becomes narrow (Bozbey, et al. 2003). In our work, all devices showed similar behavior for transition width, which is about 2K so the effect of transition width on the response couldn't be investigated.

The responsivity is linearly proportional to the dR/dT value and higher response can be observed at higher dR/dT values. On the other hand the dR/dT value increases with the bias current value since it is at the limits of thermal joule heating range. As it will be explained in the next part, the linearity of amplitude of response with the dR/dT values is well defined for devices in chip B_1. Moreover the dR/dT measurements can tell us whether response is bolometric or not. In order to show the type of response, amplitude of response versus temperature (A-T) measurements are also needed. The peaks of dR/dT and A-T measurements have to overlap; otherwise the response type will be non-bolometric. In our case there is no non-bolometric behavior because of having epitaxial films, as it explained in the second chapter.

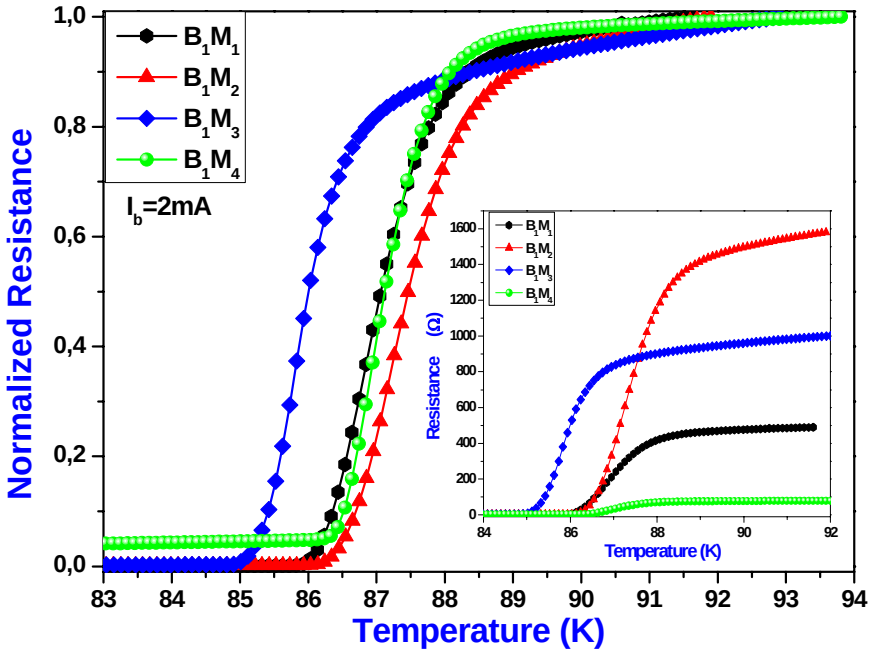

Figure 4.3. Normalized resistance versus temperature measurements of device B_1, un-normalized scale is shown in the inset figure.

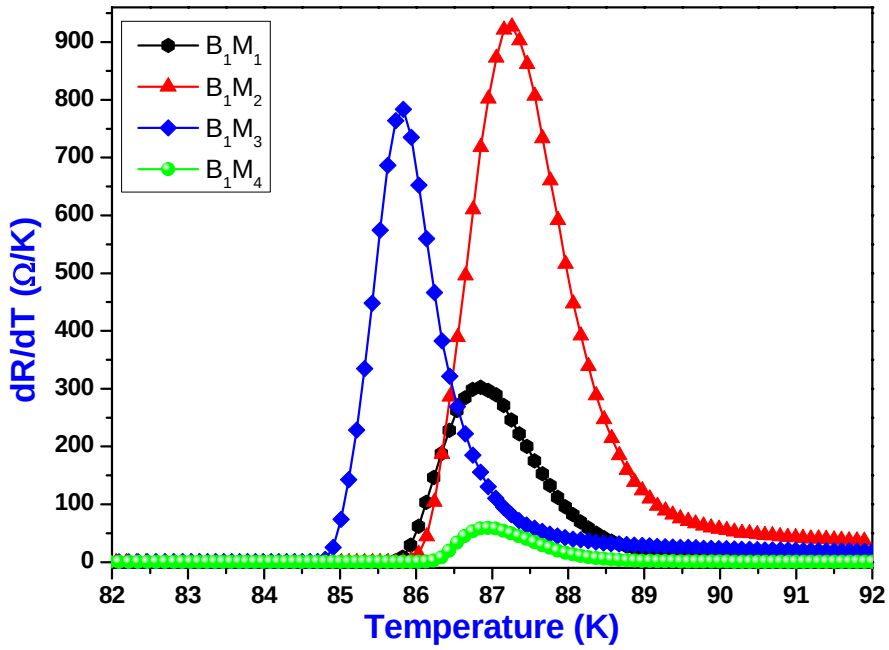

Figure 4.4. The dR/dT versus temperature for chip B_1, the data was calculated from R-T measurements.

Table 4. 1. The electrical properties and physical dimensions of chip B_1 which consist of 300nm thickness

DeviceCode*	Area of Meander line	A(mm^2)	dR/dT(Ω/K)	R(Ω)	T_c(K)	ΔT (K)
B_1M_1	30µm x 10mm	0.3	302.4	80.2	86.85	2.3
B_1M_2	30µm x 20mm	0.6	926.85	606.4	87.26	2.5
B_1M_3	50µm x 20mm	1	783.7	380.3	85.8	2.1
B_1M_4	50µm x 10mm	0.5	59.32	29.3	86.9	1.9

*The substrate material MgO, dimensions; 10x10x0.5mm

4.2.1.2. R-T for Chip B_2

The B_2 chip had lanthanum aluminate ($LaAlO_3$) as substrate and was patterned into four devices. We have just characterized two devices in this chip (B_2) which is thin (B_2M_2) and thick (B_2M_4) width and both of them have almost same area (table 4.2). The other two devices (B_2M_1 and B_2M_3) couldn't be characterized because of having very low transition temperature that our system cannot measure (liquid nitrogen, 77K). We

conclude that the reason of very low transition temperature that can be loss oxygen value of YBCO which is a common problem and also the film could have been damaged during photolithography process.

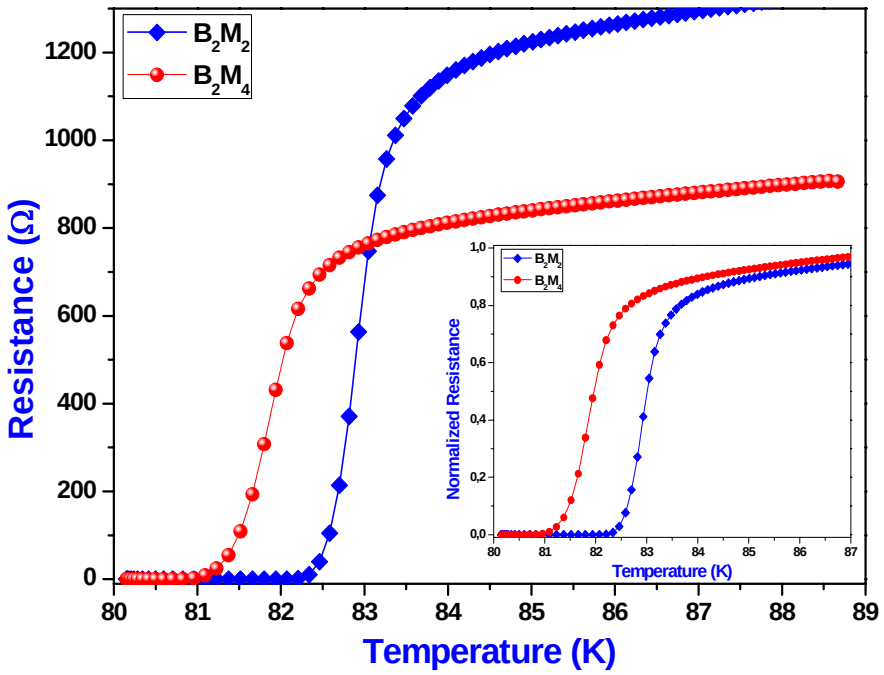

Figure 4. 5. Resistance versus temperature (R-T) measurements for chip B_2 and the inset figure shows the normalized resistance versus temperature.

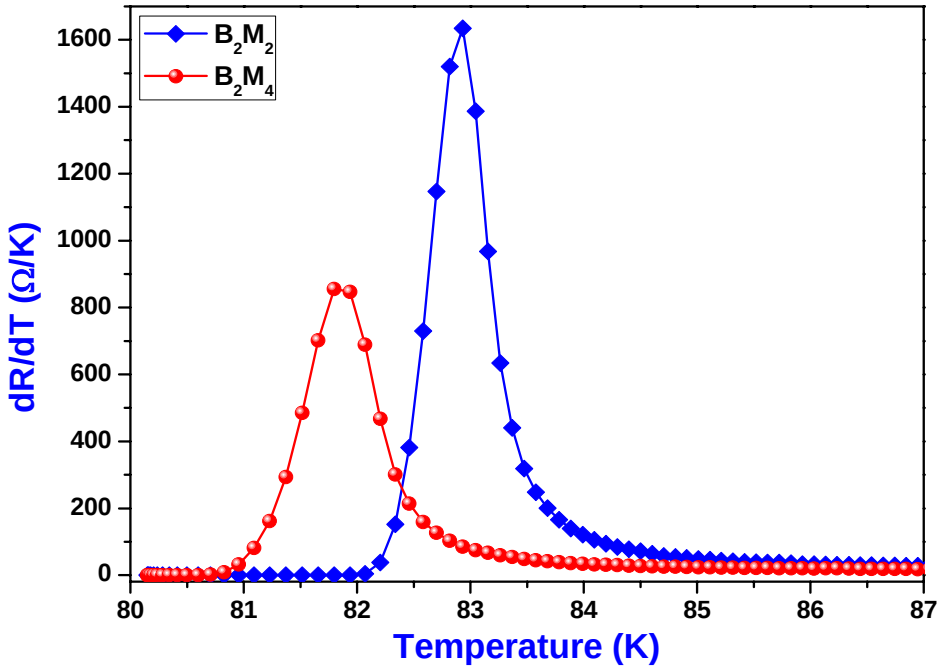

Figure 4. 6. The dR/dT versus temperature for chip B_2, the data in figure was calculated from resistance versus temperature measurement.

The R-T and dR/dT-T results are shown in the figure 4.5 and figure 4.6 respectively. The patterned devices on this chip have lowest transition temperature (T_c) when compared to the other chips (B_1 and B_3), this was also interpreted as loss of oxygen during photolithographic process or it can be due to the driving high bias current during measurements, which create a joule heating and also cause to oxygen loss. In addition, the devices on chip B_2 have sharp transitions, having ΔT's of 1.5 K for device B_1M_2 and 1.6 K for B_2M_4. Hence the dR/dT peak value of B_2M_2 is about two times greater than B_2M_4 and also the dR/dT peak value of device B_2M_2 has the greatest value among all devices that we measured.

Table 4. 2. The electrical properties and physical dimensions of chip B_2 which consist of 200nm thickness

DeviceCode*	Area of Meander line	A(mm^2)	dR/dT(Ω/K)	R (Ω)	T_c K)	ΔT(K)
B_2M_2	30μm x 20mm	0.6	1633.98	563.79	82.93	1.4
B_2M_4	50μm x 10mm	0.5	855.43	307.42	81.79	1.6

*The substrate material $LaAlO_3$, dimensions; 10x10x0.5mm

4.2.1.3. R-T for Chip B_3

The 200nm YBCO film grown on $SrTiO_3$ was patterned into four individual devices and we have characterized two devices on this chip (B_3M_2 and B_3M_3). The R-T and dR/dT characterization of these devices are shown in the figure 4.7 and figure 4.8 respectively. Actually the R-T results of these devices shows interesting behavior because of having small resistance. Especially the resistance of device B_3M_3 shows very little decreasing behavior at the temperature greater than $T_{c\text{-onset}}$ while the resistance of the other device (B_3M_2) is curved at the vicinity of $T_{c\text{-onset.}}$ Accordingly, these behaviors appear at the dR/dT graph. Moreover the superconducting transition width of devices is about 1K (see table 4.3). During etching process of this chip a very thin YBCO layer appeared at the off region of meanders so electrical short occurred in both electrical and bolometric characterizations. The small dR/dT values are undesirable because response is linearly proportional to dR/dT.

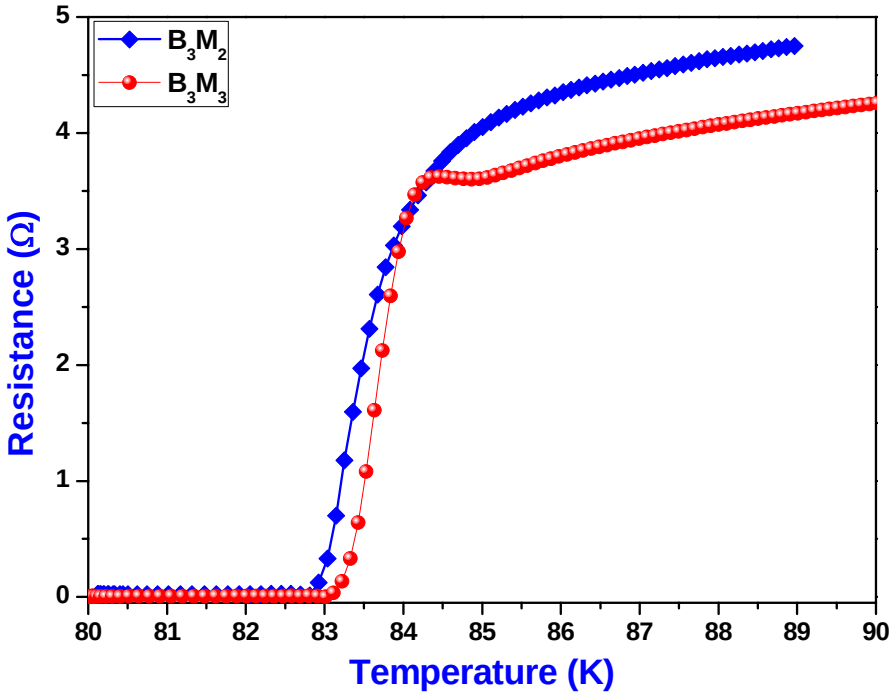

Figure 4.7. Resistance versus temperature (R-T) measurements for chip B_3 which is consist of 200nm YBCO film on $SrTiO_3$

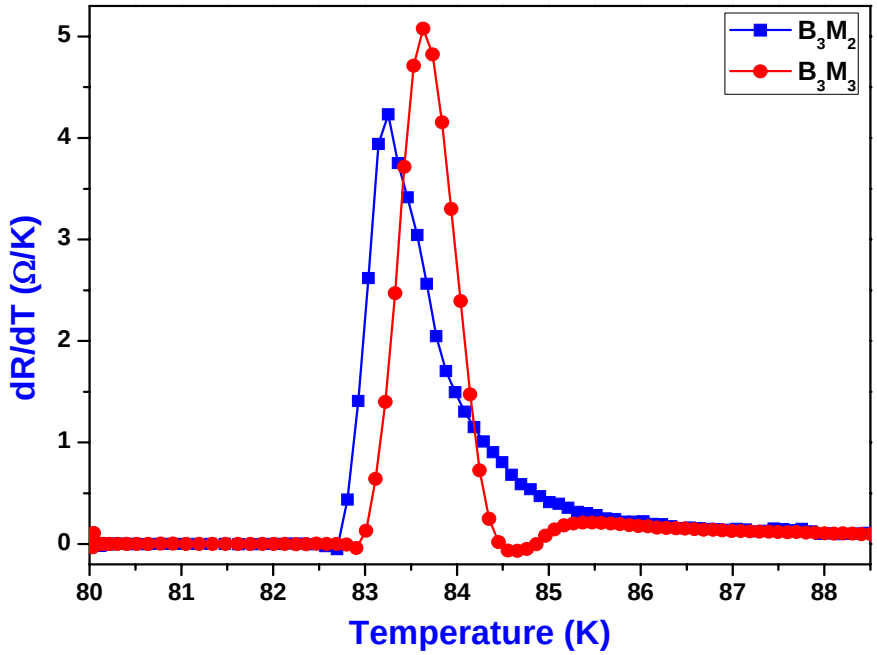

Figure 4.8. The dR/dT versus temperature for chip B_3, the data in figure was calculated from resistance versus temperature measurement in the figure 4.7.

Table 4. 3. The electrical properties and physical dimensions of chip B_3 which consist of 200nm thickness.

Device Code*	Area of Meander line	A (mm^2)	dR/dT (Ω/K)	R (Ω)	T_c (K)	ΔT (K)
B_3M_2	30 μm x 18 mm	0.54	4.23	1.18	83.25	1.8
B_3M_3	30 μm x 18 mm	0.54	5.08	1.61	83.63	1.1

*The substrate material $SrTiO_3$, dimensions; 10x10x0.5mm

4.2.2. Amplitude of Response versus Temperature Measurement Results

Amplitude of response versus temperature (A-T) measurement results constitutes one of the most important parts of this work. The performance characterizations of TEBs provide the knowledge of response voltage (in the case of current bias) at a constant frequency. As will be mentioned in the following parts, the figures of merit of the devices are measured or calculated at some constant frequency The A-T measurement results tell us a specific temperature where the response voltage is highest as well as dR/dT. Moreover, the peak point of A-T result gives the knowledge of response type, i.e. whether it is bolometric or not.

4.2.2.1. A-T for Chip B_1

In these measurements the radiation was chopped at 40 Hz constant chopping frequency in order to compare all devices in chip B_1. The chopping frequency has to be different than 50 Hz and its multiples because the measurement electronics work at 50 Hz.

We have performed A-T measurements for chip B_1 and results are given in figure 4.9. The large area devices (B_1M_2 and B_1M_3) have larger response than small area devices (B_1M_1 and B_1M_4). The results are not surprising because the dR/dT values of large area devices were higher than those with small areas (figure 4.4). Large area can

absorb more radiation than small area and therefore the radiation can create more resistance. The response voltages of large area devices are about a hundred times larger than small area devices. The response signal of large are devices are about 0.5 and 0.4 mV while small area devices have 0.006 and 0.003mV.

The responsivity is defined as the voltage signal per incident power of radiation $R_v = V_s / P$, where V_s and P are signal voltage and input power due to the radiation respectively. We have measured the radiation power of our Stephan-Boltzmann lamp by power spectrometer as mentioned in the previous chapter. The magnitude of input power is 28.8μW. By definition, the responsivity of the devices on chip B_1 can be easily calculated for 40Hz constant chopping frequency and the responsivity results are shown in the table 4.4. Moreover the responsivity of devices is calculated from simple RC model but the magnitude of responsivity from the model is higher than the magnitude of measured responsivity. Although there is a huge difference between them, the general trend remains same by means of the responsivity comparisons of large and small area devices. Furthermore, the model contains lots of parameters that we did not measure such as absorption coefficient which was assumed to be unity and linearly dependent on responsivity. In contrast, the absorption coefficient of monolithic YBCO bolometers is about 0.25 or less (Moftakharzadeh 2008). In addition of absorption coefficient, another reason of huge difference between measured and calculated responsivity is due to radiation power, although we have measured the radiation power by radiation powermeter, this can not gives us actual value because it is not easy to well align the radiation through the powermeter's detector and also align on the meander. The reason also can largely affect the responsivity because it is also linearly proportional to the voltage amplitude. It can be noted that, this huge difference was observed in all devices and the reason is the same as in this chip. The other figures of merit for this chip will be calculated in the following sections.

In addition to these measurements we have showed that the response is bolometric as shown in the figure 4.10. The peaks of A-T and dR/dT measurements are perfectly overlapped which is the clear evidence of bolometric response instead of non-bolometric one. Actually the mechanism of bolometric response is not complicated and it can be easily proven by this method. On the other hand, the non-bolometric response mechanism is too complicated and it is not easy to explain with theoretically because it depends on many parameters such as flux flow and flux creep. It appears in the

materials which contain grain boundaries which behave as Josephson junctions (Frankel 1993). The situation is very different in our devices because our devices patterned on epitaxial YBCO material and there is no Josephson junction behavior (see XRD results).

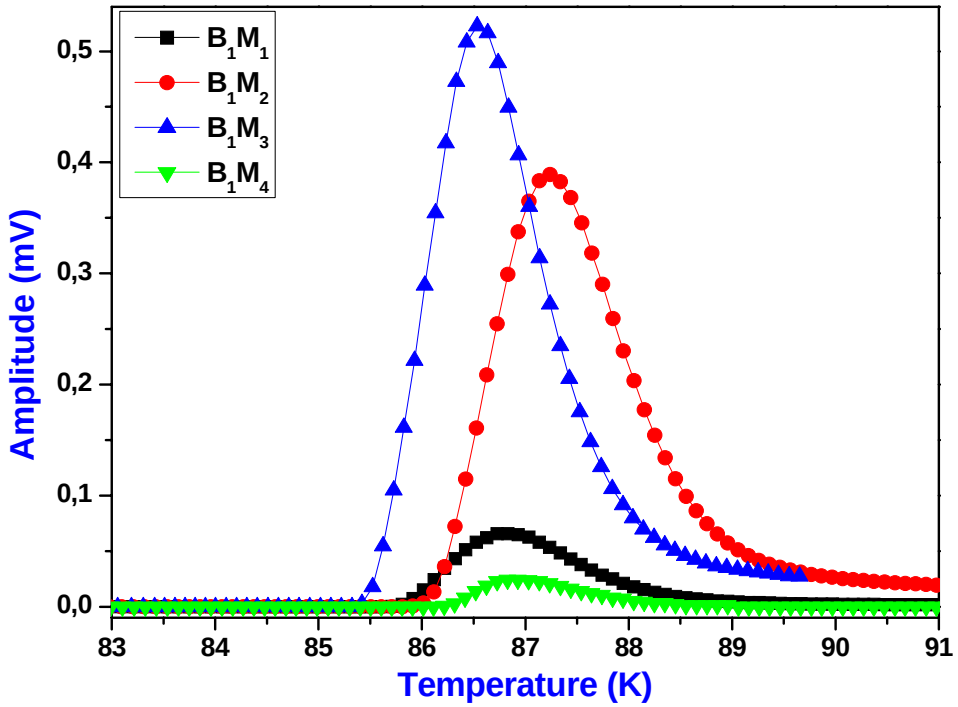

Figure 4.9. The Amplitude versus Temperature measurement at 40 Hz chopping frequency and 2mA constant bias current for chip B_1 including four devices.

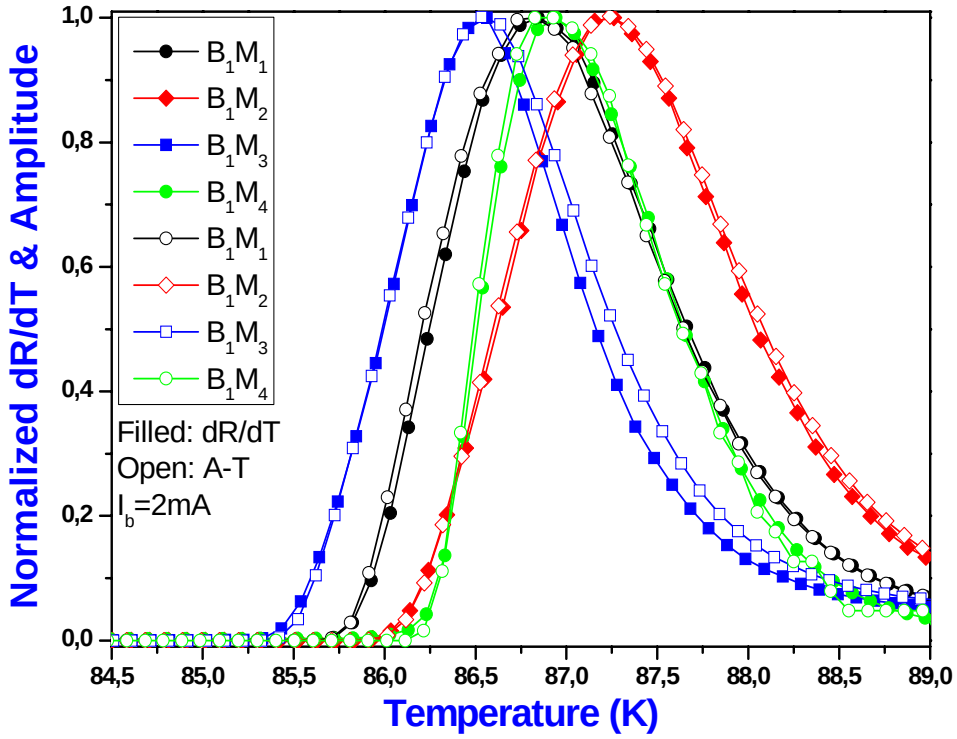

Figure 4. 10. Normalized dR/dT and Amplitude measurement for chip B1, the overlap of both peaks show that the responses are bolometric.

Table 4. 4. The measured and calculated responsivity of chip B_1

Device Code	Measured Responsivity (V/W)	RC Model (V/W)
B_1M_1	2.19	34.56
B_1M_2	12.96	41
B_1M_3	17.43	131
B_1M_4	0.8	19

4.2.2.2. A-T for Chip B_2

The A-T measurement of chip B_2 was performed for two devices having different lengths and almost the same area. The length of B_2M_2 is two times greater than the device B_2M_4 while the area of device B_2M_2 is 0.6 mm^2 and B_2M_4 is 0.5mm^2 (see table 4.2). The amplitude of response for device B_2M_2 was found to be about ten times that of device B_2M_4. The responsivity calculated with the same method as mentioned for

chip B_1 and the results are given in the table 4.4. It is calculated from simple RC model and the results also given in the same table. We have also found more contradicting results between measured and calculated results for this chip. The dR/dT measurements for this chip (figure 4.6) confirm the responsivity which was calculated from the model because dR/dT is linearly dependent on responsivity so the responsivity result of device B_2M_2 has to be larger than the device B_2M_4. We have also found a huge difference between measured and calculated results as in chip B_1, the reason of this huge difference is the same as mentioned for chip B_1 (radiation power and absorption coefficient). In addition of the A-T measurement we also showed that the response is bolometric as shown in the inset figure of 4.11.

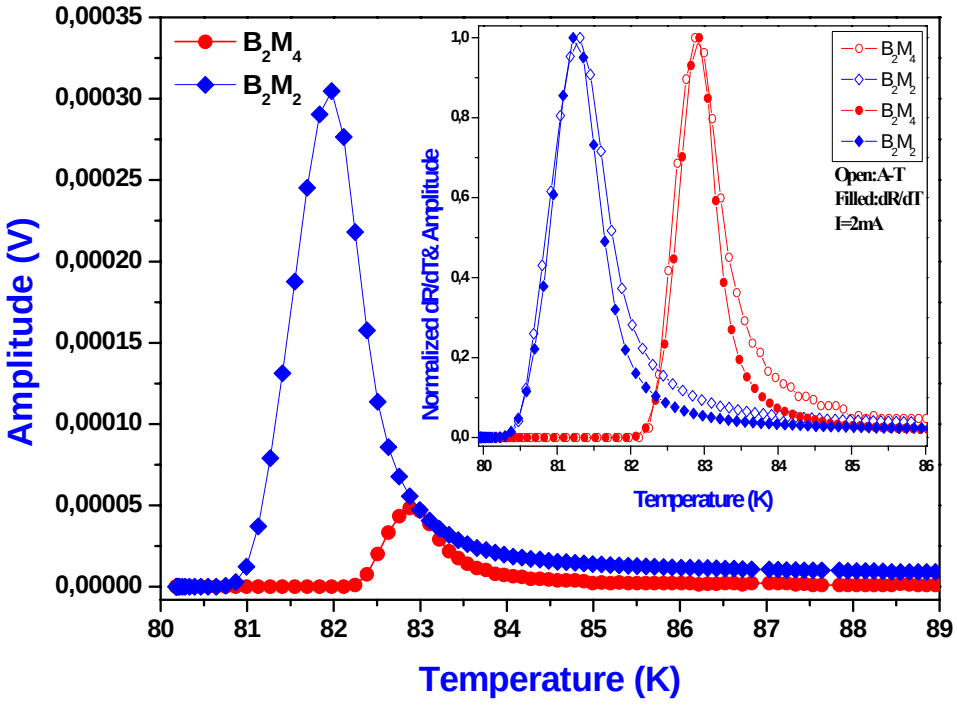

Figure 4. 11. The Amplitude versus Temperature measurement at 40 Hz chopping frequency and 2mA constant bias current for chip B_2 for device B_2M_2 and B_2M_4, the inset is normalized amplitude and dR/dT versus temperature in order to show bolometric response.

Table 4. 5. The measured and calculated responsivity of chip B_2.

Device Code	Measured Responsivity (V/W)	RC Model (V/W)
B_2M_2	10.6	346
B_2M_4	1.7	135

4.2.2.3. A-T for Chip B_3

The A-T measurement of chip B_3 is shown in the figure 4.12. The measurements were carried out at 2mA constant bias current and 20Hz chopping frequency. The chip was patterned for four identical devices and we have performed the result of two devices as shown in the figure 4.12. There is no huge difference between these two devices by means of amplitude of response as well as dR/dT measurement. However, the response voltage signals are very small due to having small resistance when it compared to the other devices. Actually this chip wasn't well etched so a very thin YBCO layer remained on the substrate which is caused to electrical short between devices and substrate. However we observed a small optical response. The A-T measurement of this chip was performed via 0.95mW HeNe laser. The measured and calculated responsivity results are shown in the table 4.5. Although there is no big difference between the responsivity of devices the measured and calculated results are very different. The reasons are the same as chip B_1.

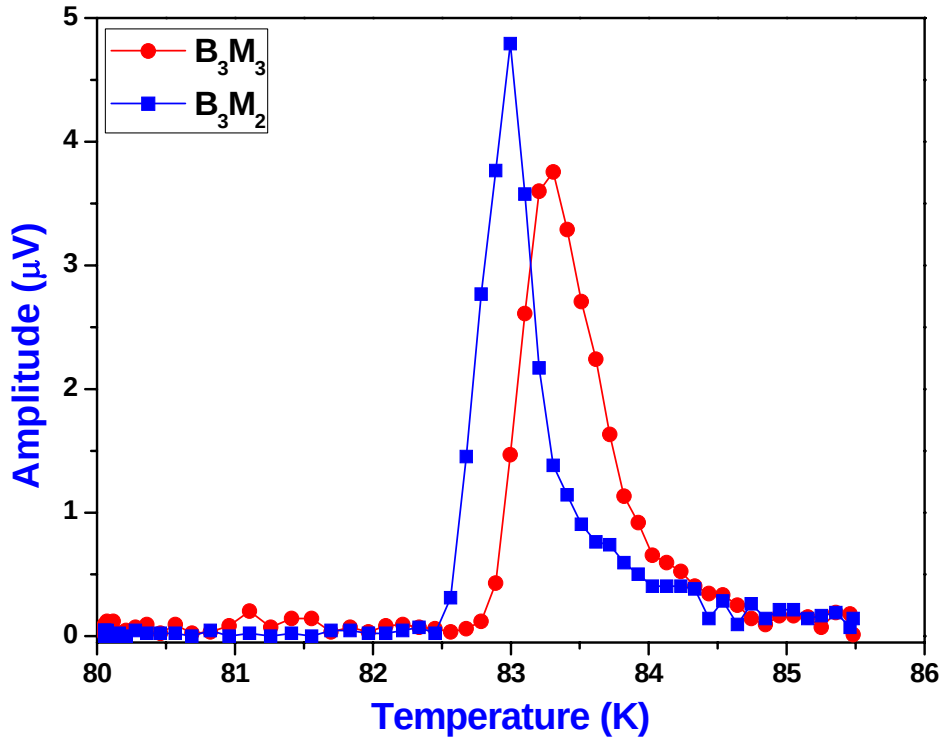

Figure 4. 12. The Amplitude versus Temperature measurement at 20 Hz chopping frequency and 2mA constant bias current for chip B_3 for device B_3M_2 and B_3M_3.

Table 4. 6. The measured and calculated responsivity of chip B_3.

Device Code	Measured Responsivity (V/W)	RC Model (V/W)
B_3M_2	5.0E-3	470
B_3M_3	4.0E-3	450

4.2.3. Amplitude of Response versus Frequency Measurement Results

The amplitude of response versus frequency measurement (A-F) is the final part of bolometric characterization. In this part, the response analysis as a function of chopping frequency was investigated and after that the results of some devices were fitted to the simple RC model as it mentioned in the 2nd chapter. Although the model explains well the low frequency regimes, the amplitude of response in high frequency regimes cannot be characterized with this model (Fardmanesh, et al. 1995). In our case we have just performed amplitude versus chopping frequency in low frequency regimes due to limitation of mechanical chopper which has a maximum chopping frequency is 550Hz. In this regime the heat flows through the substrate to the cold head and the effect of substrate/cold head interface thermal resistance (called "Kapitza boundary resistance") becomes dominant instead of film/substrate interface, substrate's or film's thermal resistance. Moreover thermal diffusion length from the surface of the film to the end point of substrate is much higher than that of substrate thickness. Therefore, in all measurements for this work only the substrate/cold head thermal boundary resistance was taken into consideration and it was measured with the joule heating method as mentioned in the previous chapter. However the effect of thickness of the devices cannot be characterized due to the limitation of mechanical chopper.

4.2.3.1. A-F for Chip B_1

The first A-F characterization for chip B_1 which include four devices was carried out at a constant temperature which is the peak point of dR/dT-T and A-T measurements and constant bias current, the result is shown in the figure 4.13. The

graph was plotted with raw data and it can be clearly seen there is no temperature fluctuation behavior; this was achieved with a good temperature stability which is about $\pm 2mK$. The response amplitude is well ordered as in the dR/dT as well as A-T measurement because of linearly dependencies (see figure 4.4 and 4.9). In the frequency regime where the measurements was carried out, the amplitude of response decreases with $f^{-1/2}$ which is the slope of the curves. Moreover the response amplitude of devices decreases when chopping frequency increases due to decreasing of thermal diffusion length of devices. In order to observe thermal diffusion length which is smaller than substrate thickness, high chopping frequencies (order of kHz) are required .

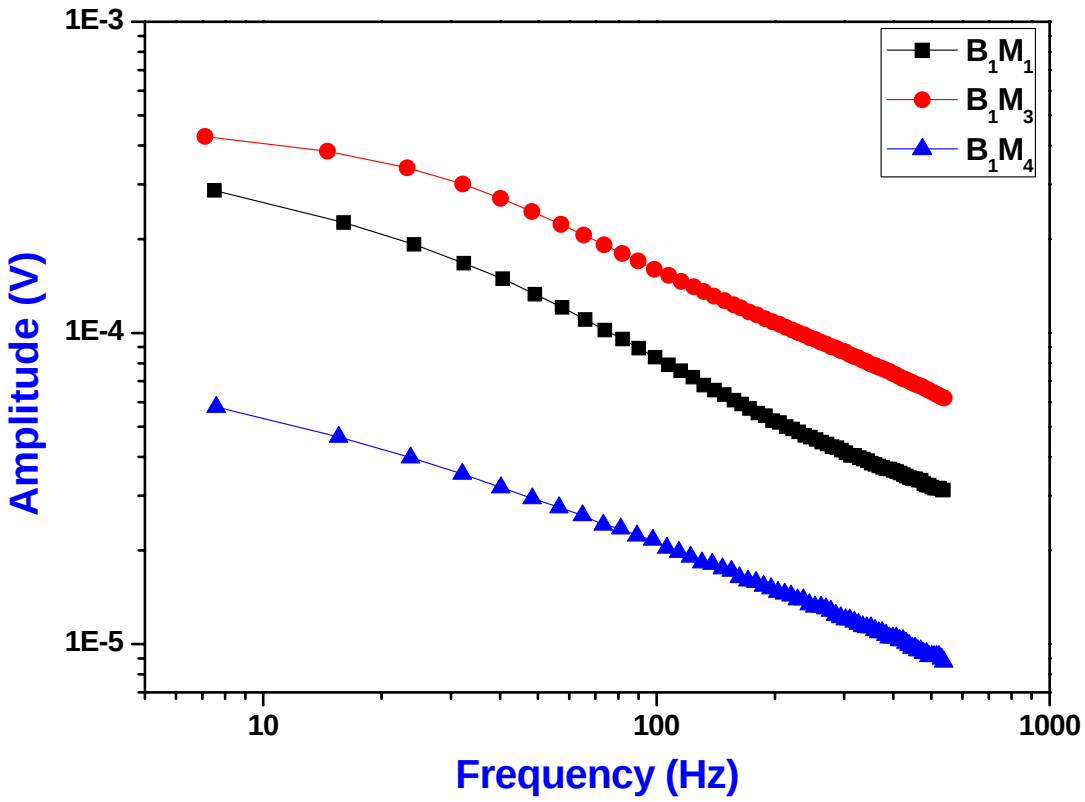

Figure 4. 13. The Amplitude of response versus chopping frequency measurement for chip B_1 (the axis are in the logarithmic scale)

In addition to the A-F measurements, we have used RC model in order to compare theoretical behavior and measured results. We aimed to get a rough idea of the behavior of our devices. For this purpose we have chosen the device B_1M_3 and the fitting result is shown in the figure 4.14. In order to fit the measured result to the RC model we have chosen absorption coefficient and the other parameters are also kept

constant except chopping frequency which we have used η for fitting variable. As it can be clearly seen in the figure the result is good agreement with the RC model.

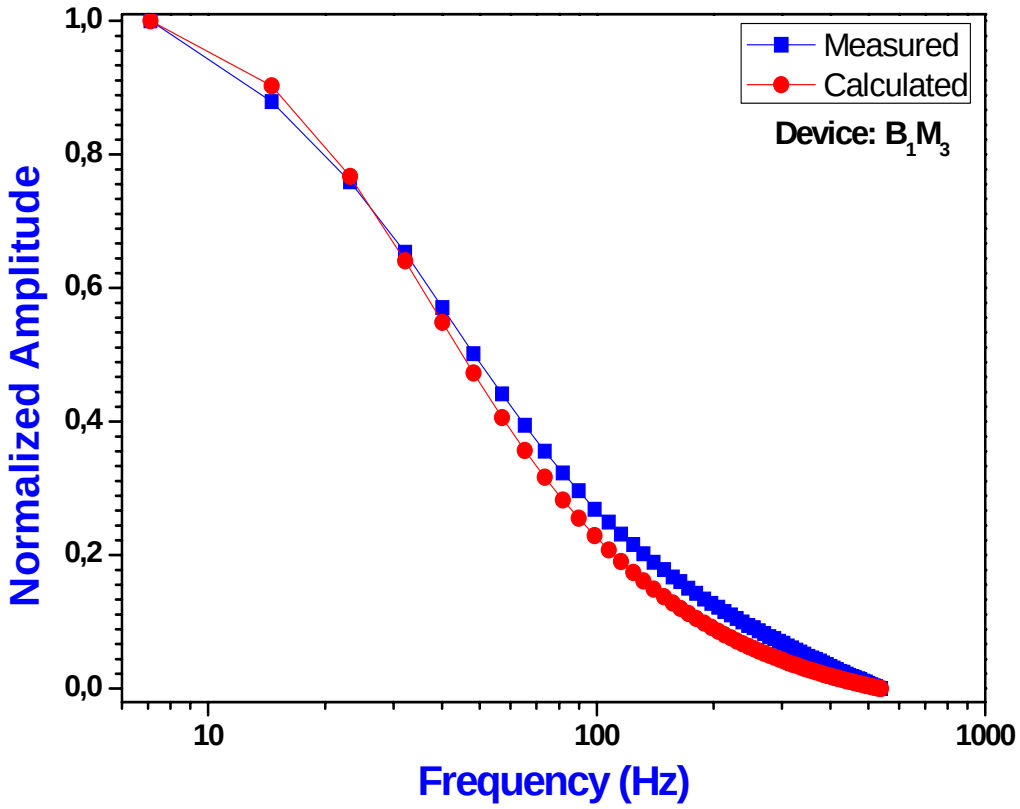

Figure 4. 14. The normalized amplitude of response versus chopping frequency result for device B_1M_3 is compared to the RC model (the x-axis is in the logarithmic scale)

4.2.3.2. A-F for Chip B_2

The A-F characterization was continued with the chip B_2 which consist of two devices and the measurement results are shown in the figure 4.15. The fitting result for device B_2M_4 is shown in figure 4.16. In the A-F measurements knee frequency can be observed at the 65Hz for both devices. The knee frequency for 0.5 mm $LaAlO_3$ substrate has calculated and found 70Hz (Fardmanesh, et al. 1995). The result is acceptable according to the theoretical calculation of knee frequency. The response amplitude value for device B_2M_2 was found 0.4mV at 7Hz and 0.012mV at 532Hz also

for device B_2M_4 0.7mV at 8Hz and 0.05mV at 533Hz. Moreover the response voltage of B_2M_2 decreases faster than device B_2M_4 at high frequency region.

The device B_2M_4 was fitted by RC model and it is also in good agreement with the model but the knee frequency was not observed in the model because of taking thermal conductance as a constant parameter instead of frequency dependent.

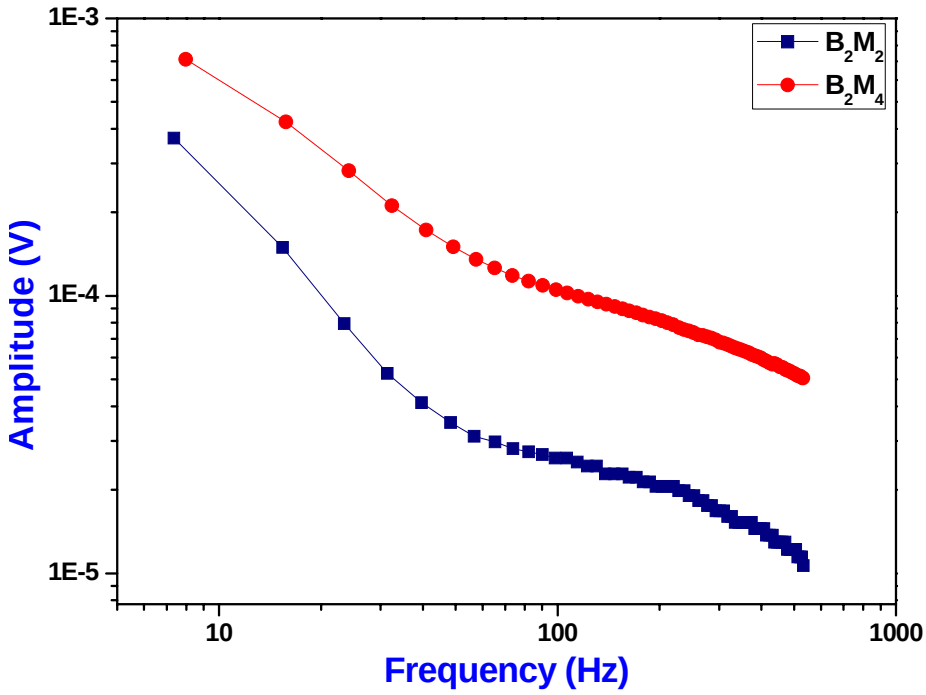

Figure 4. 15. The Amplitude of response versus chopping frequency measurement for chip B_2 (the axis are in the logarithmic scale).

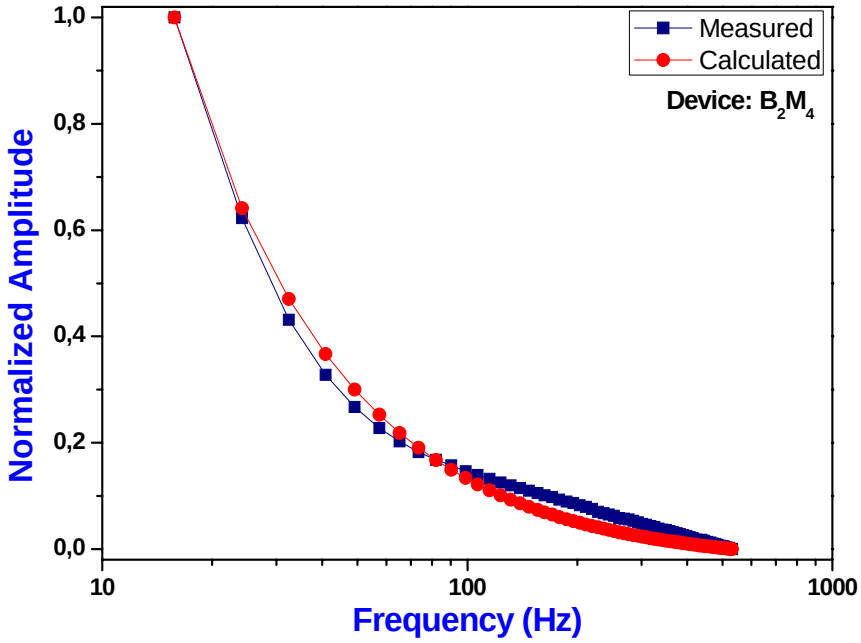

Figure 4. 16. The normalized amplitude of response versus chopping frequency result for device B_2M_4 is compared to the RC model (the x-axis is in the logarithmic scale)

4.2.3.3. A-F for Chip B_3

The A-F measurement was completed with chip B_3 which was patterned for four identical devices and one of two devices characterized via 0.95mW HeNe laser and the result for this device is shown in the figure 4.17. The response amplitude of the devices showed noisy behavior after 100 Hz chopping frequency even after the measurements were repeated. The R-T measurement of these devices also showed anomaly such as very low resistance and resistance drop at the onset temperature (see figure 4.7). These can be the reasons for noisy behavior at high frequency. The calculated knee frequency is 15.4 Hz (Fardmanesh, et al. 1995) for 0.5mm thick $SrTiO_3$ substrate but our chopper is not stable at this low frequency region so it is not easy to observe "knee" at this frequency regime. Nevertheless at the 40 Hz frequency something like knee frequency is observed for both devices but we are not sure. In addition we have applied RC model to device B_3M_3 as shown in the figure 4.18. Although below 100 Hz frequency the model is not well fitted, the frequency above 100Hz model is well behaved.

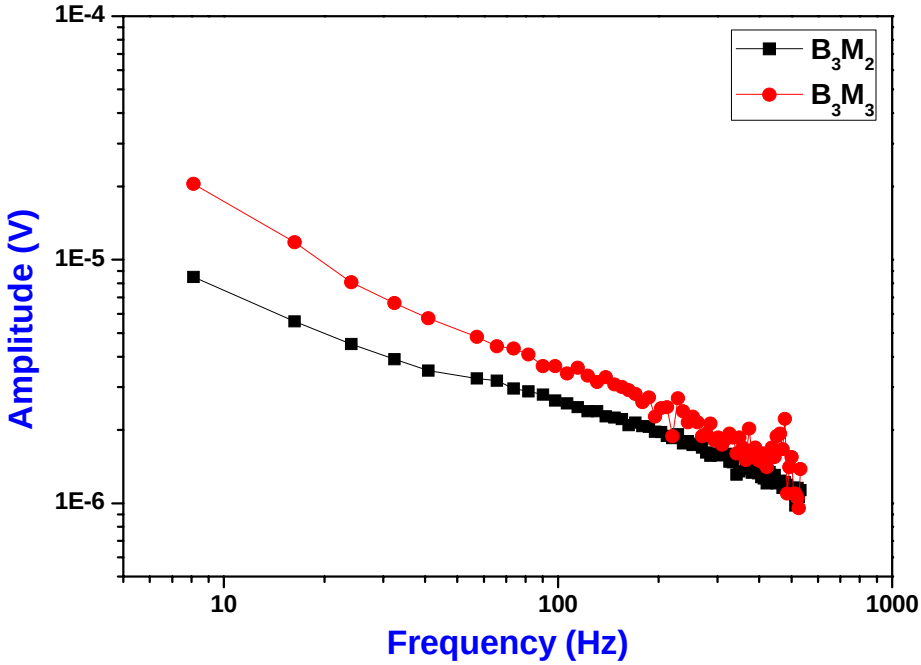

Figure 4. 17. The Amplitude of response versus chopping frequency measurement for chip B_3 (the axis are in the logarithmic scale).

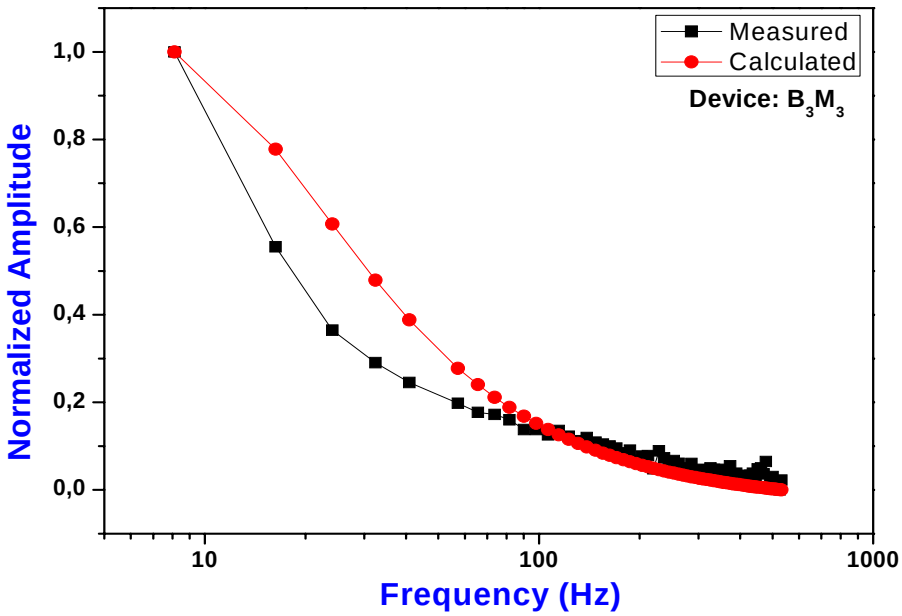

Figure 4. 18. The normalized amplitude of response versus chopping frequency result for device B_3M_3 is compared to the RC model (the x-axis is in the logarithmic scale)

4.2.4. Noise Measurements

Noise measurement is a common problem for device application and it is not easy to measure and interpret due to having complex microstructural behaviors in the crystals. In this work we have used a conventional method for measuring noise and we aimed that getting a rough idea for noise equivalent power (NEP) which is crucial importance for detector performance characterization but it is not adequate. In order to measure noise we have used a lock-in amplifier (Stanford Research System SR830) and measurements were performed at a constant frequency such as 40Hz for $LaAlO_3$, MgO and 20Hz for $SrTiO_3$. Moreover lock-in amplifier can measure noise in 1 Hz frequency bandwidth. Actually lock-in amplifier gives a noise signal in the $V/Hz^{1/2}$ quantity and we divide it by the responsivity which is calculated from basic definition as mentioned in the previous section.

In this work we have measured noise signal voltage for chip B_1, B_2 and B_3 and the results are acceptable when compared to the literature because the NEP for monolithic (bare) thick substrate bolometer is the range of 10^{-6}-$10^{-11}W/Hz^{1/2}$, for thinned or membrane substrate bolometers are in the range of 10^{-8}-$10^{-13}W/Hz^{1/2}$ and for micromachinned substrates are 10^{-10}-$10^{-12}W/Hz^{1/2}$ at about 10Hz chopping frequency (Kreisler and Gaugue 2000, Li et al. 1993, Nahum et al. 1991, Hu and Richards 1989).

Our measured results are given in the table 4.6. As it can be seen in the table, the $LaAlO_3$ based devices have higher noise than $SrTiO_3$ and MgO based devices. The NEP was measured by two radiation sources which are blackbody and HeNe laser. Actually the radiation source type can compensate the photon noise which is one of reason that $LaAlO_3$ based devices have higher noise and another reason is Johnson noise which is most dominant noise spectrum for TEBs. The Johnson noise is linearly dependent on the device resistance. Therefore due to having high resistance, $LaAlO_3$ based devices the noise appeared high.

Table 4. 7. The noise equivalent power (NEP) measurement results for chip B_1, B_2 and B_3.

Sample Code	Substrate	Radiation Source	NEP ($W/Hz^{1/2}$)
B_1M_1	MgO	Black Body @ 40Hz	$7.4*10^{-9}$
B_2M_2	LaAlO3	Black Body @ 40Hz	$\sim10^{-7}$
B_2M_4	LaAlO3	Black Body @ 40Hz	$\sim10^{-7}$
B_3M_2	SrTiO3	HeNe Laser @ 20Hz	$\sim1.2*10^{-8}$
B_3M_3	SrTiO3	HeNe Laser @ 20Hz	$\sim1.2*10^{-8}$

4.2.5. Detectivity Calculations

Detectivity was defined in the last part of the second chapter. Based on the definition, the detectivities of chip B_1, B_2 and B_3 were calculated with the knowledge of NEP. The $LaAlO_3$ based devices detectivities have about $\sim10^6 cmHz^{1/2}/W$ while $SrTiO_3$ and MgO based devices have higher detectivity values as in the order of $\sim10^7 cmHz^{1/2}/W$. In addition the detectivity calculations were carried out at a constant frequency which was 40Hz for chip B_1, B_2 and 20Hz for chip B_3. Actually the detectivity of our devices is not so high, possiblu due to all monolithic YBCO based devices .The limitation of absorption can be overcome by coating absorption layer which is also not so easy due to having instability of YBCO material.

Table 4. 8. The detectivity (D^*) calculation results for chip B_1, B_2 and B_3.

Sample Code	Substrate	Radiation Source	D^* ($cmHz^{1/2}$/ W)
B_1M_1	MgO	Black Body@40Hz	$0.7*10^7$
B_2M_2	LaAlO3	Black Body@40Hz	$0.8*10^6$
B_2M_4	LaAlO3	Black Body@40Hz	$0.7*10^6$
B_3M_2	SrTiO3	HeNe Laser@20Hz	$0.6*10^7$
B_3M_3	SrTiO3	HeNe Laser@20Hz	$0.6*10^7$

Table 4. 9. The performance comparison of our devices (B_1M_1, B_2M_2 and B_3M_2) with literature.

	Our Devices			**Literature**		
	MgO	**LAO**	**STO**	**MgO***	**LAO****	**STO*****
Responsivity (V/W)	2.19	10.15	$5*10^{-3}$	10@10Hz	3.2@10Hz	<<1
NEP ($W/Hz^{1/2}$)	$7.4*10^{-9}$	10^{-7}	10^{-8}	$3.9*10^{-8}$	$1.9*10^{-8}$	10^{-6}@17Hz
D^*($cmHz^{1/2}/W$)	$0.7*10^{7}$	$0.8*10^{6}$	$0.6*10^{7}$	$1.5*10^{7}$	$\sim10^{7}$	10^{6}

* Eidelloth 1991, ** Moftakharzadeh et al. 2008 and *** Leung et al. 1987

Table 4.8 shows performance comparison of our devices with literature for thick substrate bolometers. As it can be seen in the table the noise equivalent power (NEP) of our devices by means of sensitivity is in good agreement with the literature and our MgO and STO based substrate devices are 10 times smaller (better) than chosen literature values. In addition the detectivity of our devices also have better or same values when compared to the literature values put in the table. Actually, responsivity could be studied further because it can be increased by some convenient ways such as coating and antenna coupling. This can be future work of this study.

CHAPTER 5

CONCLUSION

Thermal detectors have been investigated since 1800s. Due to having a long research history of thermal or radiation detectors, many applications have been carried out such as thermal imaging, particle detection and astronomical research. Actually the physics of sensors is not too easily understandable because of their complex mechanism. The detector application in the field of superconducting material is not too old. The first superconducting detector was discovered in 1938, while high temperature superconducting detectors were developed in 1980s.

We have produced, characterized and analyzed monolithic large area YBCO epitaxial thin film transition edge bolometers. The YBCO thin films are grown on three different substrates which are MgO, $LaAlO_3$ and $SrTiO_3$. Our YBCO thin films were purchased from a commercial company and were fabricated with two different surface qualities." The structural characterizations were performed by x-ray diffraction (XRD) and scanning electron microscopy (SEM). The XRD results showed that our films are epitaxial and c-axis oriented, which is important in observing bolometric response. The SEM results give us knowledge about surface morphology and the best surface morphology was observed for $SrTiO_3$ substrate which is "S" type film.

The work in this thesis started with patterning of thin films. The film grown on MgO and $LaAlO_3$ substrates were patterned into four different devices while $SrTiO_3$ was patterned into four identical devices. However two of the patterned devices on $LaAlO_3$ substrate was not characterized due to having low superconducting transition temperatures which were below the liquid nitrogen temperature (77K). Two of the devices on the $SrTiO_3$ substrate also were not characterized because of having the same properties with other devices on $SrTiO_3$.

After structural characterization, electrical characterizations such as resistance versus temperature (R-T), amplitude of response versus temperature (A-T) and amplitude of response versus chopping frequency (A-F) were carried out. The R-T characterization is of crucial importance for transition edge bolometers (TEBs).

Therefore we have measured the R-T of thin films accurately by slowly increasing the temperature. The R-T results of MgO based devices showed expected results. The longer (large area) devices have larger resistance than shorter (small area) devices and their dR/dT results followed this ordering also. As the responsivity of the devices is proportional to the dR/dT values, higher dR/dT values is preferred. This linearity was confirmed by amplitude of response versus temperature (A-T) results. Higher dR/dT resulted in a higher response amplitude. In addition, the A-T and dR/dT measurement results perfectly overlapped, which is the evidence of bolometric response rather than non-bolometric response in the measurement times we employed. The bolometric characterization of MgO based devices were continued with amplitude of response versus chopping frequency (A-F) measurements and these results were compared to the RC model. The A-F results of MgO based devices were fitted to the model and we showed that our result is well explained with the model.

The same measurements for MgO based devices were performed for both $LaAlO_3$ and $SrTiO_3$ based devices. The R-T results of $LaAlO_3$ based devices have the highest dR/dT values when compared to other devices. In addition the A-F measurements were performed and the results were fitted to the RC model as before. The results show that the model explains the behavior of B_1 well. However it has higher NEP when compared to the other devices, possibly because Johnson noise is linearly dependent on the resistance. High NEP also causes low detectivity value. The $LaAlO_3$ based substrate showed low performance when compared to the other chips.

The $SrTiO_3$ based devices have the lowest responsivity due to having very small dR/dT values. The chip was not well etched and a very thin YBCO layer was remaining on the STO substrate, causing electrical short between layer and patterned devices. It can be noticed that TEBs need to be well processed in order to get a high response. Although the measured responsivity was small, the calculated responsivities of the devices on this chip have very large values. In our calculations, before normalization, the radiation absorption coefficient was taken to be unity initially, leading to a huge apparent disparity between the theoretical and observed results. When the theory was normalized to the results, excellent fits were obtained, suggesting low absorption coefficients. The normalization factors were as low as 5% to 10%. A 10% to 20% factor was expected, as this value corresponds to the absorption coefficient of YBCO found in literature. The reason for even lower observed coefficients could include the

measurement method of the radiation power.We have just measured the magnitude of radiation power by a radiation power meter but it is not easy to measure radiation power by this way. Another reason for the disparity could be that the alignment of blackbody radiation through the detector is not exact. The infrared lasers are more convenient ways to characterize TEBs, but when TEBs are used in the field, they will be detecting blackbody (or graybody) radiation rather than laser..

There's a tradeoff in the design of the devices between responsivity and speed. Given a certain bolometer architecture, increased speed leads to a decreased responsivity. Therefore, given a bolometer architecture, beyond improving the fabrication methods, a compromise needs to be made. Which point this compromise needs to be made at would depend on the application area of the bolometer.

After electrical and bolometric characterization, we have measured the noise performance of our devices by lock-in amplifier. The noise measurements were carried out at a constant frequency and we aimed to get a rough idea about the noise performance. Although the noise measurements require more sensitive measurement methods such as the use of a spectrum analyzer, our results are also acceptable when compared to the literature. We have measured the noise voltage of MgO, $LaAlO_3$ and $SrTiO_3$ based devices at 40 Hz and 20 Hz constant chopping frequencies respectively. The noise measurement of MgO, $LaAlO_3$ based devices was performed with black body radiation while $SrTiO_3$ based devices was performed with HeNe laser. After that we have calculated the noise equivalent power (NEP) of our devices by the definition as mentioned in the 2nd chapter. The NEP result of $SrTiO_3$ based devices showed smaller (better) values than $LaAlO_3$ based devices. In the noise figures of $LaAlO_3$, it is possible that the Johnson noise becomes dominant because the Johnson noise is linearly dependent on resistance and $LaAlO_3$ based device has very large resistance at the operating temperature when compared to the $SrTiO_3$ devices. On the other hand the MgO based device showed best sensitivity and detectivity. As I mentioned before, although a high dR/dT value can produce a high response, it can also cause high Johnson noise, hence low sensitivity. We have also calculated the detectivity of $LaAlO_3$ and$SrTiO_3$ devices by the knowledge of NEP. The results are not perfect but they can be acceptable when compared to the literature because the maximum detectivity performance of monolithic bolometers is the order of ~10^{10}cm$Hz^{1/2}$/W in the microwave region.

The work is completed but some more investigations can be carried out. In order to explore the effect of thickness of the films on the responsivity of our devices, high chopping frequency is needed. However mechanical choppers are limited to low frequencies and hence they contain wobble,creating extra noise. This problem can be overcome via a TTL modulated laser. Advanced thermal models found in literature can be applied to the results. In addition, in order to get a response from higher wavelength regimes such as mid to far infrared regimes, radiation coupling and membrane type bolometers are needed. The substrate of the bolometer used in this thesis can be thinned by wet etching or by ion milling. If available, micromachining technology can be used with similar purposes. Furthermore, investigations can be performed with antenna coupled or composite bolometers. By these methods the performance of bolometers as given by NEP and detectivity (D) can be improved.

REFERENCES

Abrikosov, A.A. 1950. Magnetic properties of superconductors of the second group. *Sov. Phys. JETP* (Engl. Transl.), Vol/Issue: 5:6.

Anderson, Philip Warren. 1997. *The Theory of Superconductivity in High T_c Cuprates*. New Jersey: Princeton University Press.

Avci, I. 2007. Fabrication and Applications of High-Tc YBCO DC-SQUID Magnetometers. *Ege University Thesis of PhD*.

Ayache, J. 2006. Grain boundaries in high temperature superconducting ceramics, *Phylosophical Magazine*. Vol. 86, No. 15, 2193-2239.

Bardeen, J., L.N. Cooper, and J.R. Schrieffer 1957. Microscopic Theory of Superconductivity. *Phys. Rev*. 108, 1175 – 1204.

Bednorz, J.G., K.A. Muller, M. Takashige 1987. Superconductivity in Alkaline Earth-Substituted La_2CuO_{4-y}. *Science,* Vol. 237. no. 4819, pp. 1133 – 1139.

Brasunas, J. C., S. H. Moseley, B. Lakew,R. H. Ono, D. G. McDonald, J. A. Beall, and J. E. Sauvageau 1989. Construction and performance of a high-temperature-superconductor composite bolometer. *J. Appl. Phys*. 66, 4551.

Bozbey, A. 2006. Investigation, Modeling, and Applications Feasibility of the Thermal Crosstalk in High Tc Transition Edge Bolometer Arrays. *Bilkent University Thesis of PhD*.

Bozbey, A. 2003. YBCO Transition Edge Bolometers: Effect of Superconductivity Transition on the Phase and Magnitude of Response. *Bilkent University Thesis of MS.*

Bozbey, A., M. Fardmanesh, I.N. Askerzade, M. Banzet and J. Schubert 2003. Effects of the superconductivity transition on the response of YBCO edge transition bolometers. *Supercond. Sci. Technol.* 16 1554-1558.

Clarke, J., P. L. Richards, and N.H. Yeh 1977. Composite superconducting transition edge bolometer. *Appl. Phys. Lett*. 30, 664.

Dereniak, E.L. and G.D. Boreman 1996. *Infrared detectors and system*. Canada: John Willy & sons, inc.

Duzer,T.V. 1999. *Principles of superconductive devices and circuits*, Berkeley: Prentice-Hall.

Eidelloth, W. 1991. Optical response of highly oriented YBCO thin films. *IEEE Trans. Magn*. 27 2828.

Fardmanesh, M., K. J. Scoles, and A. Rothwarf 1999. Control of the responsivity and the detectivity of superconductive edge-transition Y Ba2Cu3O7-δ bolometers through substrate properties. *Appl. Optics*, vol. 38, no. 22, pp.4735.

Fardmanesh, M., A. Rothwarf, K.J. Scoles 1995. Low and midrange modulation frequency response for YBCO infrareddetectors: interface effects on the amplitude and phase. *IEEE Trans. on Appl. Superconductivity*, vol. 8, no. 1.

Fardmanesh, M., A. Rothwarf, K. J. Scoles 1995. $YBa_2Cu_3O_{7-\delta}$ Infrared Bolometers: Temperature Dependent Responsivity and Deviations From The dR/dT curve, *Journal of applied physics*, vol. 77, no:9, pp. 4568-4575.

Fardmanesh, M. A. Rothwarf and K.J. Scoles 1996. Noise Characteristics and Detectivity of YBCO superconducting Bolometers: Bias Current, Frequency and Temperature Dependence. *J.Appl.Phys.* 79 (4).

Fardmanesh, M., M. Ihsan, K.J Scoles and A. Rothwarf 1993. Thin Film YBCO infrared Detector Design and Characterization. BFS Center - *Superconductivity and Its Applications*: Buffalo, NY 1992, Amer Inst of Physics.

Farrell, D. E., J. P. Rice and D. M. Ginsberg, 1990. Experimental evidence for flux-lattice melting. *Phys. Rev. Lett*. 67, 1165 – 1168.

Frenkel, A. 1993. Mechanism of nonequilibrium optical response of high-temperature superconductors. *Phys.Rev.B*, Vol. 48, No. 13.

Ginzburg, V.L., L.D. Landau 1950. On the theoryof superconductivity. *Zh. Eksperim. i Teor. Fiz*.

Hao, J.H., F.Q. Zhou, X.R. Zhou, H.D.Sun, X.J.Yi, Z.G. Li 1993. Responsivity calculation and measurement of YBCO optical detector. *IEEE Transections on Applied Superconductivity*, Vol.3, No.1.

Herwaarden, A.W. V., D.C.V. Duyn, B.W.V. Oudheusden 1989. Integrated Thermopile Sensor, *Sensors and Actuators*, xensor.nl.

Hu, Q. and P.L. Richards 1989. Design analysis of a high Tc superconducting microbolometer, *Appl.Phys.Lett*. 55 (23).

Irwin, K.D. 1995. An application of electrothermal feedback for high resolution particle detection. *Appl.Phys.Lett.* 66 15, pp.1998-2000.

Ivanov, K.V., D.A. Khokhlov, I.A. Khrebtov, Yu.V. Kulikov, V.G. Malyarov, A.D. Nikolenko, V.F. Pindyurin and V.Yu. Zerov 2007. Characterization of the composite bolometer with a high-T_c superconductor thermometer for an absolute

radiometer of synchrotron radiation. *Nuclear Instruments and Methods in Physics Research A* 575 272-275.

Izumi, F., E. Takayama-Muromachi 1995. Crystal structures and phase equilibria, *High-Temperature Superconducting Materials Science and Engineering*, *Pages 81-130.*

Kadin, A.M. 1999. *Introduction to superconducting circuits*. Canada: John-*Wiley*.

Ketterson, J.B., S.N. Song 1999. *Superconductivity*, Cambridge: Cambridge University Press.

Kittel, C. 1976. *Introduction to Solid State Physics*. California: *Wiley*.

Kraus, H. 1996. Superconductive Bolometers and calorimeters. *Supercond. Sci. Technol*. 827-842.

Kreisler A.J. and A. Gaugue 2000. Recent progress in high-temperature superconductor bolometric detectors: from the mid-infrared to the far-infrared (THz) range. *Supercond. Sci. Technol.* 13 1235-1245.

Kruse, P.W. 1990. Physics and application of high temperature superconductors for infrared detectors. *Semicond. Sci. Technol*. 5 S229-S239.

Khrebtov, I. A. 2002. Noise properties of high temperature superconducting bolometers. *Fluctuation and Noise Letters*, Vol.2, No.2, R51-R70.

Khrebtov, I.A., AD Tkachenko 1999. High-temperature superconductor bolometers for the IR region. *Journal of Optical Technology*, OSA.

Lakew, B., J.C. Brasunas, S. Aslamb, D.E. Pugel, 2004. High-Tc, transition-edge superconducting (TES) bolometer on a monolithic sapphire membrane-construction and performance. *Sensors and Actuators A,* 114 (2004) 36–40.

Lambkin, P., N. Folan, B. Lane 1999. Simple Technique for the measurement of Thermal time constants of microbolometer structures. *Proc.IEEE Int. Conf. on Microelectronic test structures,* Vol.12.

Lee, S.F., J.M. Gildemeister, W. Holmes, A. T. Lee, P.L. Richards 1998. Voltage-biased superconducting transition-edge bolometer with strong electrothermal feedback operated at 370 mK, *APPLIED OPTICS,* Vol. 37, No. 16-OSA.

Leung, M., P. R. Broussard, J. H. Claassen, M. Osofsky, S. A. Wolf, and U. Strom 1987. Optical detection in thin granular films of Y-Ba-Cu-O at temperatures between 4.2 and 100 K. *Appl. Phys. Lett.* 51, 2046

Li, K., Joseph E. Johnson, Bruce W. Aker 1993. High responsivity $YBa_2Cu_3O_{7-x}$ microbolometers with fast response times. *J. Appl. Phys*. **73**, 1531.

Loram, J.W., K.A. Mirza, J. R. Cooper, and W.Y. Liang 1993. Electronic specific heat of $YBa_2Cu_3O_{6+x}$ from 1.8 to 300 K. *Phys. Rev. Lett.* 71, 1740.

Meissner, W. and R. Ochsenfeld 1933. Ein neuer Effekt bei Eintritt der Supraleitfähigkeit. *Naturwissenschaften* 21, 787.

Méchin, L., J. C. Villégier, P. Langlois, D. Robbes and D. Bloyet 1996. Sensitive IR bolometers using superconducting YBaCuO air bridges on micromachined silicon substrates. *Sensors and Actuators A: Physical* ,Volume 55, Issue 1, Pages 19-23.

Mischke, M. 2003. Wavelength Dependence of the Photoresponse of a Yittirium-Barium-Copper-Oxide Thin Film. *Notre Dame University Thesis of PhD.*

Moftakharzadeh, A., A. Kokabi, A. Bozbey, T. Ghods-Elahi, M. Vesaghi, S. Khorasani, M. Banzet, J. Schubert, and M. Fardmanesh 2008. Detectivity of YBCO transition edge bolometer: modulation frequency, bias current and absorber effects. *Journal of Physics: Conference Series* 97 012009.

Nahum, M., Q. Hu, P.L. Richards 1991. Fabrication and measurement of high Tc superconducting microbolometers, *IEEE Trans. Magn.* MA6-27,308l.

Nahum, M., S. Verghese, P. L. Richards, K. Char 1991. Thermal boundary resistance of Y Ba2Cu3O7-δ Films. *Appl. Phys. Lett*, vol. 59, no. 16, pp. 2034.

NASA 2000. Earth Observatory archive. http://www.earthobservatory.nasa.gov (Accessed 7 October 2008)

Nivelle, M. J. M. E., M. P. Bruijn, R. de Vries, J. J. Wijnbergen, and P. A. J. de Korte, S. Sa ´nchez, M. Elwenspoek, T. Heidenblut, B. Schwierzi, W. Michalke, E. Steinbeiss. 1997. Low noise high-Tc superconducting bolometers on silicon nitride membranes for far-infrared detection. *J. Appl. Phys*. 82 (10), 15.

Prasher, R.S., P.E. Phelan 1997. Review of thermal boundary resistance of high-temperature superconductors. *Journ. of Supercond*. Vol. 10, No. 5, pp473-484.

Rahman, F. 2006. Superconducting detectors in astronomy. *Contemporary Physics*, Volume 47, Number 4, Julyâ, pp. 181-194(14).

Richards, P. L.1994. Bolometers for infrared and millimeter waves. *J. Appl. Phys.* 76, 1.

Richards, P.L., J. Clarke, R. Leoni, P.H. Lerch, S. Verghese, M.E. Beasley, T.H. Geballe, R.H.Hammond, P.Rosenthal, S.R.Spielman 1989. Feasibility of the high T superconducting bolometer. *Applied Physics Letters*, 54, 283.

Robbes, D., N. Cheenne, J.F. Hamet, J.P. Rice 1999. Thermal boundary resistance of a $YBa_2Cu_3O_{7-\delta}$/$SrTiO_3$multilayer strip. *IEEE Transactions on Applied Superconductivity*, Volume: 9, Issue: 2, Part 3, On page(s): 3874-3877.

Slack, G.A. 1962. Thermal Conductivity of MgO, Al_2O_3, $MgAl_2O_4$, and Fe_3O_4 Crystals from 3° to 300°K. *Phys. Rev*. 126, 427 – 44.

Szentpali, B. 2007. Noise limitation of the Application of Miniature Thermal resistors. *IEEE Sensors Journal*, Vol. 7, No. 9.

Tinkham, M. 1996. *Introduction to superconductivity*. New York: McGraw-Hill.

Tseng, T.Y., C.Y. Chang, C.J. Haung, M.C. Chen 1991. Bolometric YBCO infra-red detector. *Electronics Letters*, Vol.27, No.19.

Omar, M.A. 1993. *Elementary Solid State Physics: Principles and Applications*. Michigan: Addison-Wesley Pub. Co.

Uher, C., AB Kaiser, 1987. Thermal Transport Properties of YBa2Cu3O7 Superconductors. *Phys. Rev. B, Condens Matter*, Volume 36 Issue 10.

Verghese, S., P. L. Richards, K. Char, D.K. Fork, T.H. Geballe 1992. Feasibility of infrared imaging arrays using high-T, superconducting bolometers. *J. Appl. Phys.* 71, 2491.

Verghese, S., P. L. Richards, K. Char and S.A. Sachtjen 1991. Fabrication of an infrared bolometer with a high Tc superconducting thermometer. *IEEE Transactions on Magnetics,* Volume: 27, Issue: 2, Part 4, 3077-3080.

Vincent, J.D. 1989. *Fundamentals of Infrared detector Operation and Testing*. WileyBlackWell.

Werner, B. 1991. *Superconductivity: Fundamentals and Applications*. *VCH*.

Williams, P.J. 1993. Pair breaking effects on the specific heat of a superconductor. *Physical review B*, Vol.47, Number 22.

Wördenweber, R. 1999. Growth of high-Tc thin films. *Supercond. Sci. Technol* 12 R86.

Wu, M.K., J.R. Ashburn, C.J. Torng, P.H. Hor, R.L. Meng 1987. Superconductivity at 93 K in a new mixed-phase Y-Ba-Cu-O compound system at ambient pressure. *Phys. Rev. Lett.* 58, 908 – 910.

Yoon, J., K. Ahn, D. Youm 1999. Bolometric effects of YBCO film on a Pt membrane. *Physica C: Superconductivity* ,Volume 324, Issues 3-4, 1, Pages 143-152.